

Co-funded by the



# CEBAMA

➤ (Contract Number: **662147**)

## Deliverable n° D3.04

### Description of and results from the modelling of external lab and/or field experiments.

Editors: Andrés Idiart (Amphos 21)

Date of issue of this report: 01.12.2016

Report number of pages: 47

Start date of project: 01/06/2015                      Duration: 48 Months

Project co-funded by the European Commission under the Euratom Research and Training Programme on Nuclear Energy within the Horizon 2020 Framework Programme		
Dissemination Level		
<b>PU</b>	Public	X
<b>PP</b>	Restricted to other programme participants (including the Commission Services)	
<b>RE</b>	Restricted to a group specified by the partners of the CEBAMA project	
<b>CO</b>	Confidential, only for partners of the CEBAMA project	

## **ABSTRACT**

The present deliverable D3.04 contains a description of modelling approaches and recent progress by WP3 partners and summarizes the results of the modelling of existing experimental datasets. Given that experimental results in CEBAMA will become available later in the project, preliminary work in WP3 has thus been focused on the development and implementation of models and on the simulation of existing experimental datasets.

Each partner contribution below summarizes the modelling work so far, with application to existing experiments, using a similar approach to the one proposed to analyse experimental data generated in CEBAMA. In some cases, the efforts so far have been devoted mainly to the development of the modelling tools.

---

## 1 KIT/ V. Montoya

### Abstract

Coupled reactive transport modelling will be applied for interpretation of the experimental results of WP1 and WP2. Experimental work within these two WP includes through diffusion experiments of HTO,  $^{36}\text{Cl}^-$ ,  $^{129}\text{I}^-$ , and Be across the interface between bentonite porewater and low-pH cement. Given that all the experimental results will become available later in the project, work in WP3 has been focused so far on a) the development of the conceptual model for modelling the experimental results of the CEBAMA project and b) the implementation/application of models to the simulation of existing experimental datasets.

### 1.1 INTRODUCTION

KIT-INE is mainly interested on quantifying and modelling the precipitation/dissolution process in the interface between cementitious materials and porewaters with different compositions. Thermodynamic modelling is used as a first approach to predict the dissolution and precipitation of secondary phases. Later, the models have incorporated and taken into account the coupling between porosity changes due to dissolution/precipitation and its effect on radionuclides migration. The experimental results of the CEBAMA project will be modelled with a newly developed code/interface called iCP (Nardi et al. 2014), which couples two different codes: the Finite Element code COMSOL Multiphysics V.5 (COMSOL 2014) and the geochemical simulator PHREEQC v.3.1.1.7. (Parkhurst, and Appelo, 2013).

The existing experimental dataset used for calibrating the models consist of long-term leaching/degradation of full scale cemented wastes in salt brine and tap water. Twenty-eight monoliths were investigated containing up to 10 wt.% simulated ILW from reprocessing. The waste simulate consists mainly of  $\text{NaNO}_3$  cemented waste in 200 L-scale and reacted in NaCl-rich and  $\text{MgCl}_2$ -rich brines over 20 to 35 years. Additionally, few drums were also put in contact with tap water. The samples were doped with cesium-137, uranium and neptunium-237. An ordinary Portland cement (OPC CEM I 42.5 R) with water to cement (w/c) ratios ranging from 0.235 to 0.50 L/kg were used to test the behaviour of real scale, simulated, cemented waste forms with respect to chemical resistance and radionuclide mobilization (Kienzler et al. 2016, Borkel et al. 2017).

The modelling work has been used to simulate:

- the cement degradation and
- the radionuclide mobilization/retention.

### 1.2 CEMENT DEGRADATION

Thermodynamic equilibrium calculations were performed for modelling the cement degradation in contact with the brine waters. The software ‘The Geochemist’s Workbench’ (GWB) (Bethke and Yeakel, 2009) was used as tool for thermodynamic modelling. GWB uses a logK approach (equilibrium constants) to calculate a system’s equilibrium state from a selected (or individually compiled) thermodynamic database allowing any supersaturated minerals to precipitate. The thermodynamic data were consistently compiled in a database for the calculations (Bube et al., 2013). The thermodynamic data was taken from Harvie, Møller and Weare (Harvie et al. 1984) for the oceanic salts, complemented by aquatic species of Si (Reardon, 1992) and Al (Hummel et al. 2002). The Pitzer approach (Pitzer, 1979) was used to calculate activities of aqueous species to account for the high ionic strength of the systems. The relevant Pitzer parameters were taken from Reardon (1988, 1990). Relevant solid phases were selected from several databases (Reardon, 1992,

---

Robie and Hemingway, 1995, Lothenbach and Winnefeld, 2006, Matschei et al. 2007, Stronach and Glasser, 1997, Wolery, 1997). In the case of solid solutions, ideal miscibility was supposed and the different end members were defined. The sequence of miscibility of the C-S-H solid-solutions was modelled according to Stronach and Glasser (1997) applying end members of different Ca/Si ratios. Thermodynamic datasets compiled in GWB format can be formatted to be used in other codes like PHREEQC (Parkhurst and Appelo, 2013), enabling comparison and validation of different codes.

For details of previous numerical simulation and results with monoliths #31, #32, #33, and #34, see Bube et al. (2013, 2014) and Figure 1.1. The calculated results agree well with the experimentally determined data both for full-scale block in NaCl and MgCl<sub>2</sub> solution. The agreement refers to the solution concentrations and the cement hydrates, as well as secondary phases. It was shown that the initial inhomogeneity at the surfaces of the simulate blocks did not affect the comparison between experimental and numerical data. The good agreement of results for NaCl and MgCl<sub>2</sub> systems supports the assumption that the finally measured constant concentrations of the leachates represented a state of geochemical equilibrium and were not controlled by kinetic effects.

Additionally, the modelling performed with PHREEQC 3 to analyse the change of porosity due to solid precipitation dissolution was presented in the Mechanisms and Modelling of Waste /Cement Interactions Conference held in 2016, Murten, Switzerland by Borkel et al. (See Figure 1.2).

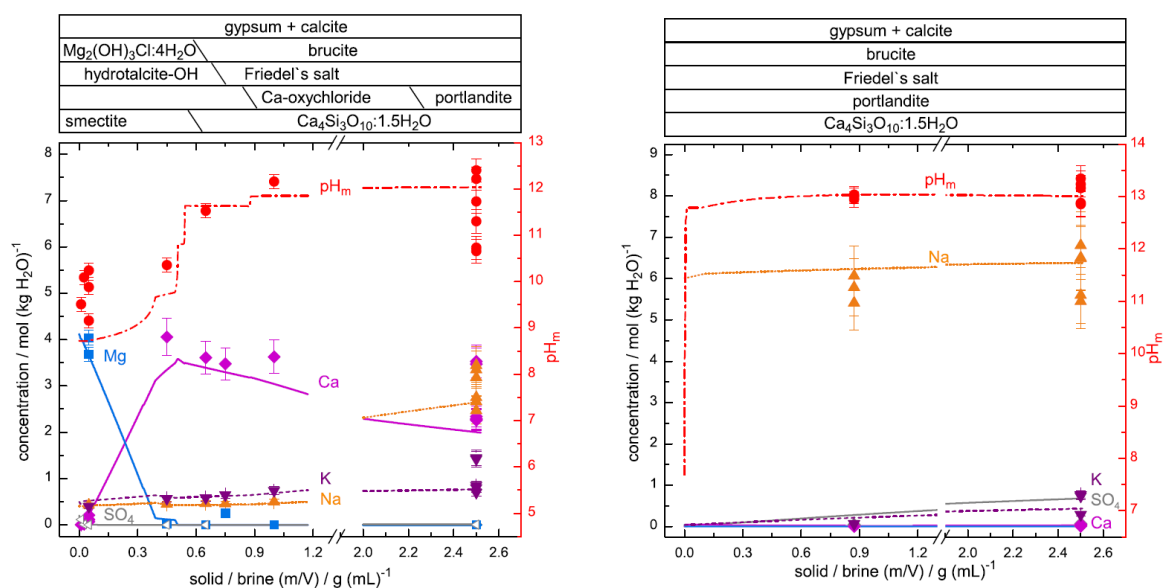


**Figure 1.1.** Calculated equilibrium concentrations and experimental steady state data of major solution components in MgCl<sub>2</sub> (left) and NaCl system (right) as function of m/V ratio (extracted from Bube et al. 2013).

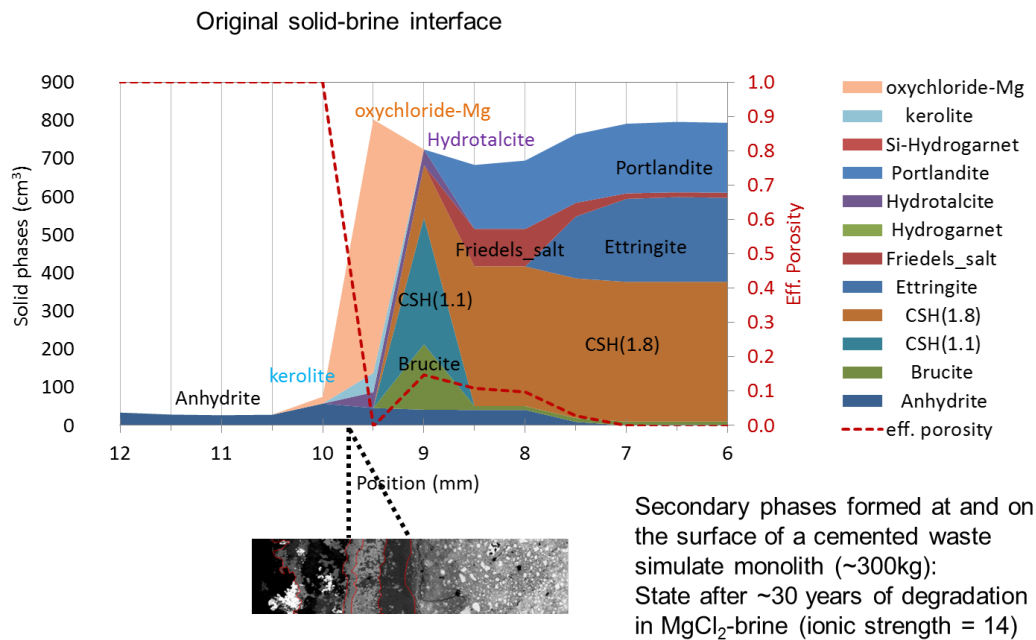


**Figure 2.2.** Modelling of the degradation process of the cemented waste simulate at low w/c ratio in MgCl<sub>2</sub> rich brines (extracted from presentation by Borkel et al., 2016).

### 1.3 RADIONUCLIDE MOBILIZATION/RETENTION

Referring to the mobilization of radionuclides, caesium migration in the cemented waste was selected to perform the modelling work. In this case, mainly diffusion controlled migration was assumed and diffusion parameters calculated. In the case of the NaCl brine system a 3D model (cylindrical geometry) was implemented in the FlexPDE-finite element software (PDE Solutions Inc.). Calculations include Cs<sup>+</sup>, Cl<sup>-</sup> and NO<sub>3</sub><sup>-</sup> diffusion in the full-scale simulate blocks prepared at high W/C ratio. Details of previous models were published in Kienzler and Metz (2009). The diffusion coefficients were fitted to the measured data as a function of time. Due to the availability of experimental data for Cs, the temporal evolution of the leachate concentration was applied, while for Cl<sup>-</sup> and NO<sub>3</sub><sup>-</sup>, the measured profiles in the solid were used. Apparent diffusion coefficients for Cs<sup>+</sup>, Cl<sup>-</sup> and NO<sub>3</sub><sup>-</sup> were fitted. The modelling approach allowed to derive a sorption coefficient for caesium in the corroded cement matrix under the assumption that anions are not sorbed. The obtained value was  $K_d(\text{Cs}^+) = 0.23 \text{ ml} \cdot \text{g}^{-1}$ , which was in the expected range for Cs sorption onto cement (Jakob et al., 1999).

In the case of the leaching experiments performed with cemented simulated waste products in tap water, the code Phreeqc v3.1 (Parkhurst and Appelo, 2013) was used. In this case, the main focus is related with the leaching of Cs explained by diffusion processes (Borkel et al., 2014). In the modelling, the constraint of charge balance was stressed and results are compared to the analytical solution (see Figure 1.3).

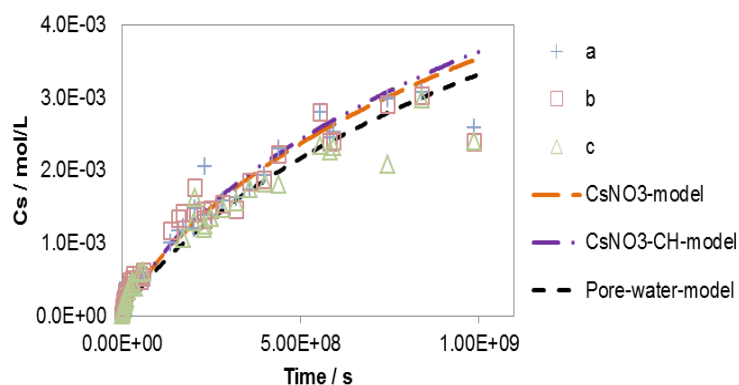


**Figure 1.3.** Cs release from cement monoliths a, b and c over 31 years compared to calculated Cs release according to the PHREEQC model with varying solution compositions. (extracted from Borkel et al., 2014).

## 1.4 REFERENCES

- Bethke C., Yeakel S. (2009). The Geochemist's Workbench, Univ. of Illinois, Urbana, USA.
- Borkel C., Montoya V., Kienzler B. (2014). Modeling long-term leaching experiments of full scale cemented wastes: effect of solution composition on diffusion, NUWCEM. CEA, Avignon, France.
- Borkel C. Schlieker M., Kienzler B., Metz V. (2017). Degradation of Real Scale Cemented Simulated Waste Forms Over 35 Years in Salt Brines. Phys. Chem. Earth. Submitted
- Bube C., Metz V., Bohnert E., Garbev K., Schild D., Kienzler B. (2013). Long-term cement corrosion in chloride-rich solutions relevant to radioactive waste disposal in rock salt – Leaching experiments and thermodynamic simulations. Phys. Chem. Earth, 64, 87-94.
- Bube C., Metz V., Schild D., Rothe J., Dardenne K., Lagos M., Plaschke M., Kienzler B. (2014). Combining thermodynamic simulations, element and surface analytics to study U(VI) retention in corroded cement monoliths upon >20years of leaching. Phys. Chem. Earth, 70-71, 53-59.
- Harvie C. E., Møller N., Weare J.H. (1984). The prediction of mineral solubilities in natural waters: The Na-K-Mg-Ca-H-Cl-SO<sub>4</sub>-OH-HCO<sub>3</sub>-CO<sub>3</sub>-CO<sub>2</sub>-H<sub>2</sub>O system to high ionic strengths at 25°C, Geochimica et Cosmochimica Acta, vol. 48, pp. 723-751.
- Hummel W., Berner U., Curti E., Pearson F.J. Thoenen T. (2002). Nagra/PSI Chemical Thermodynamic Data Base 01/01, Nagra, Wettingen, Switzerland, 1015-2636, Tech. Report, 589.
- Jakob F., Sarott A., Spieler P. (1999). Diffusion and sorption on hardened cement pastes - experiments and modelling results, PSI Report 99-05.
- Kienzler B., Borkel C., Metz V., Schlieker M. (2016). Long-Term Interactions of Full-Scale Cemented Waste Simulates with Salt Brines, KIT Scientific Reports 7721, Karlsruhe, Germany.
- Kienzler B., Metz V. (2009). Modelling long-term corrosion of cemented waste forms in salt brines, in 12th Internat. Conf. on Environmental Remediation and Radioactive Waste Management (ICEM '09), Liverpool, GB, October 11-15, 2009.
- Nardi A., Idiart A., Trincherro P., de Vries L.M., Molinero J. (2014). Interface COMSOL-PHREEQC (iCP), an efficient numerical framework for the solution of coupled multiphysics and geochemistry. Computers & Geosciences, 69, 10-21.

- Parkhurst D.L., Appelo, C.A.J. (2013). Description of input and examples for PHREEQC Version 3 - A computer program for speciation, batch-reaction, one-dimensional transport, and inverse geochemical calculations. U.S. Geol. Survey Techniques and Methods, book 6, chapter A43, 6-43A.
- Pitzer K.S. (1979). Theory: Ion interaction Approach, in Activity coefficients in electrolyte solutions. vol. 7, R. M. Pytkowicz, Ed., ed: CRC Press, INC. Boca Raton FL., 157-208.
- Reardon E. J. (1992). Problems and approaches to the prediction of the chemical composition in cement/water systems, *Waste Manag*, 12, 221-239.
- Reardon E. J. (1988). Ion interaction parameters for aluminum sulfate and application to the prediction of metal sulfate solubility in binary salt systems. *The J. of Phys. Chem.*, 92, 6426-6431.
- Reardon E. J. (1990). An ion interaction model for the determination of chemical equilibria in cement/water systems. *Cem. Concr. Res.*, 20, 175-192.
- Robie R. A., Hemingway B. S. (1995). *Thermodynamic Properties of Minerals and Related Substances at 298. 15 K and 1 bar (10<sup>5</sup> Pascals) Pressure and at Higher Temperatures*. USGS Geol. Survey Bulletin 1452.
- Lothenbach B., Winnefeld, F. (2006). Thermodynamic modelling of the hydration of Portland cement, *Cement and Concrete Research*, 36, 209-226.
- Matschei T., Lothenbach B., Glasser F. P. (2007). Thermodynamic properties of Portland cement hydrates in the system CaO–Al<sub>2</sub>O<sub>3</sub>–SiO<sub>2</sub>–CaSO<sub>4</sub>–CaCO<sub>3</sub>–H<sub>2</sub>O. *Cem. Concr. Res.*, 37, 1379-1410.
- Stronach S. A., Glasser F. P. (1997). Modelling the impact of abundant geochemical components on phase stability and solubility of the CaO–SiO<sub>2</sub>–H<sub>2</sub>O system at 25°C: Na<sup>+</sup>, K<sup>+</sup>, SO<sub>4</sub><sup>2-</sup>, Cl<sup>-</sup> and CO<sub>3</sub><sup>2-</sup>. *Advances in Cement Research*, 9, 167-181.
- Wolery T. J. (1992). EQ3/6, A Software Package for Geochemical Modeling of Aqueous Systems, University of California, Lawrence Livermore National Laboratory.
-

### Abstract

In order to assess the long-term integrity and performance of cementitious barriers for their use in underground nuclear waste disposal, the evolution of the main physical properties over time needs to be well understood. These properties can be altered by chemical reactions as a result of clay-cement interaction or the effect of groundwater. Not only the transport properties need to be estimated, but also the mechanical long-term behaviour, to ensure the mechanical stability of the repository. Calcium leaching from cement paste is generally accepted to be one of the most relevant degradation processes in the long-term for nuclear waste repositories. It is well-known that this process leads to a more porous microstructure, negatively impacting the transport and mechanical properties of concrete. To study these coupled processes, a reactive transport model is coupled to a micromechanical model to simulate a set of existing accelerated calcium leaching experiments. The impact of calcium leaching on the mechanical and transport properties is explicitly considered in the model. Simulation results are compared to recent experimental data obtained from accelerated calcium leaching experiments, showing how chemically-induced damage impacts the physical properties of cement paste and concrete.

### 2.1 INTRODUCTION AND OBJECTIVES

One of the main degradation processes expected to play a role in deep geological repositories is calcium leaching from the solid matrix of cementitious materials due to the chemical gradient between the barriers and the environment (e.g. Idiart et al., 2016). Due to the fact that this process is very slow, calcium leaching experiments are typically performed using a more aggressive leaching solution than expected under repository conditions, e.g. using deionized water or different concentrations of ammonium nitrate (Adenot and Buil (1992), Babaahmadi et al. (2015)).

The effect of calcium leaching on concrete properties is a result of the dissolution of a sequence of cement hydrates (portlandite, C-S-H gels, ettringite, etc.) leading to a more porous microstructure. As a consequence, the diffusivity and permeability can significantly increase (e.g. Camps, 2008). The mechanical properties (Young's modulus, tensile and compressive strength) can also decrease substantially (Gérard et al. (1998), Heukamp et al. (2005)).

Recently, a set of calcium leaching experiments using OPC hardened cement paste and concrete specimens has been conducted at Chalmers University of Technology in Sweden (Babaahmadi et al. (2015)). In their setup, a 0.3 M ammonium nitrate solution is used coupled to electrical migration through cement paste and concrete samples. In this way, the leaching process is substantially accelerated, enabling the use of relatively large specimens which can then be used for macroscopic characterization tests (permeability, diffusivity and mechanical properties) over the reference (i.e. intact) and aged (i.e. leached) states of the same samples. More details can be found in Babaahmadi et al. (2015) and Idiart and Coene (2016).

The model developed in this work does not intend to reproduce the accelerated experiments in terms of the time needed to reach an aged sample. The goal has been to determine, by means of reactive transport modelling, the leaching acceleration factor obtained with the experiment when compared to the leaching of the same samples subjected to groundwater interaction. Furthermore, the outcome of the model in terms of chemical and physical properties of the aged samples can be compared to the experimental data to gain insight into the mechanisms of chemical degradation when using the accelerated leaching test.

---

The chemo-mechanical model used here considers specific features of the coupling between mechanically-driven and chemically-driven damage when concrete is subject to calcium leaching. A schematic representation of the coupling between different processes considered is shown in Figure 2.1.

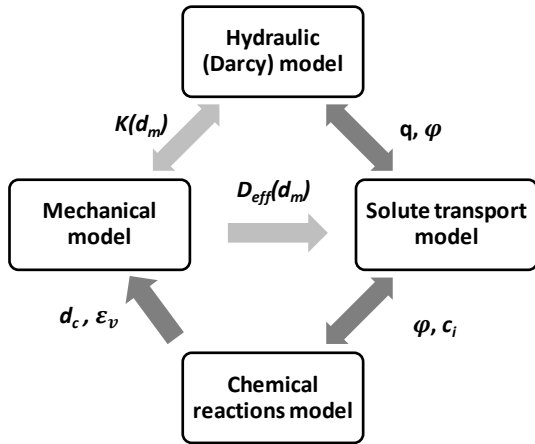


**Figure 2.1.** Schematic representation of physico-chemical couplings in the model.  $d_c$  and  $d_m$ : chemical and mechanical damage;  $\kappa(d_m)$  and  $D_{eff}(d_m)$ : empirical relations of permeability and diffusivity as a function of mechanical damage;  $q$ : Darcy velocity;  $c_i$ : species concentration;  $\varphi$ : porosity.

## 2.2 MULTI-SCALE CHEMO-MECHANICAL MODEL

A multi-scale chemo-mechanical model is implemented in iCP (interface Comsol-Phreeqc, Nardi et al., 2014) at the continuum scale, where the cementitious material is regarded as homogeneous. The model encompasses a classical reactive transport framework based on (1) solute transport and (2) chemical reactions, with (3) a non-linear damage mechanics model of the cementitious system, and (4) a multi-scale micromechanical model. The latter is used to describe the coupling between changes in the microstructure of cement paste and concrete (due to chemically-driven degradation) and the mechanical properties. The micromechanical model computes the elastic constants as a function of the volume fractions of all the minerals in concrete and is used to calculate the isotropic chemical damage,  $d_c$  (between 0 and 1). Two mechanical damage models have been implemented to calculate the isotropic mechanical damage,  $d_m$  (between 0 and 1). The constitutive models are based on Mazars' damage model (Mazars, 1986) and on the more recent  $\mu$ -model for more realistic behaviour under multiaxial compressive stresses (Mazars et al., 2015). Regularization of the models, necessary to obtain mesh-independent results, is based on a gradient-enhanced model following an implicit gradient formulation (e.g. Peerlings et al., 1996). Both damage variables are scalar and coupling of chemical and mechanical damage is considered to be multiplicative. For these experiments, solute transport is limited to Fickian diffusion, although both the diffusion coefficient and permeability are updated as a function of chemically-driven porosity changes in the model. Mineralogical, porewater, and boundary groundwater compositions in the model can be found in Idiart et al. (2016). Chemical reactions are calculated at chemical equilibrium using the thermodynamic database CEMDATA07 (Lothenbach et al. (2008)).

The multi-scale micro-mechanical model implemented in iCP is based on homogenization theory to describe the effective properties at different scales based on information about the morphology of the structure at a lower scale and the volume fractions of the different constituents. The model is based on the work by Stora et al. (2009) and Bary et al. (2014). More details can be found in Idiart and Coene (2016) and Idiart et al. (2016).

## 2.3 COMPARISON BETWEEN MODEL AND EXPERIMENTAL RESULTS

In the following, only some of the results obtained are presented. A more detailed description of the model setup and results obtained can be found in (Idiart et al., 2016, Idiart and Coene, 2016).

Comparison of model and experimental results is presented in Figure 2.2 in terms of the profile of the Ca/Si ratio along the cement paste sample axis. As the experiments were accelerated due to electrochemical migration, the corresponding model times were found by comparing the time at which portlandite was completely leached: 53 days in the experiments and 11,000 years in the model. It can be seen that the initial and final times obtained with the reactive transport model offer a good fit with the experimental results. At intermediate times the tendency is similar, but the leaching depth differs slightly.

The homogenization model for chemical damage is validated by comparing model and experimental results of the Young's modulus of the initial and leached specimens. As shown in Table 2.1, a good agreement between model and experimental results is found, both for initial and leached specimens. The main difference between experimental and modelled results is the initial Young's modulus of the HCP. A very low value (11 GPa) has been measured experimentally. However, reported experimental values by other authors at this w/c ratio and for an almost complete degree of hydration show systematically higher values, in the order of 20 GPa or more. The comparison of compressive and tensile strength of intact and aged concrete specimens is presented in Table 2.2. The evolution of the effective diffusion coefficient is also compared to experimental data in Table 2.2. The effective diffusion coefficient of the model increased from  $2.8 \cdot 10^{-12}$  to  $11.3 \cdot 10^{-12}$  m<sup>2</sup>/s due to the increase in porosity resulting from mineral dissolution. The effective diffusion values reported by Babaahmadi et al. (2015) are significantly higher (roughly by an order of magnitude) and not typical of intact concretes with similar water-to-cement ratios. However, the ratio of diffusivities between aged and intact concrete specimens are very similar.

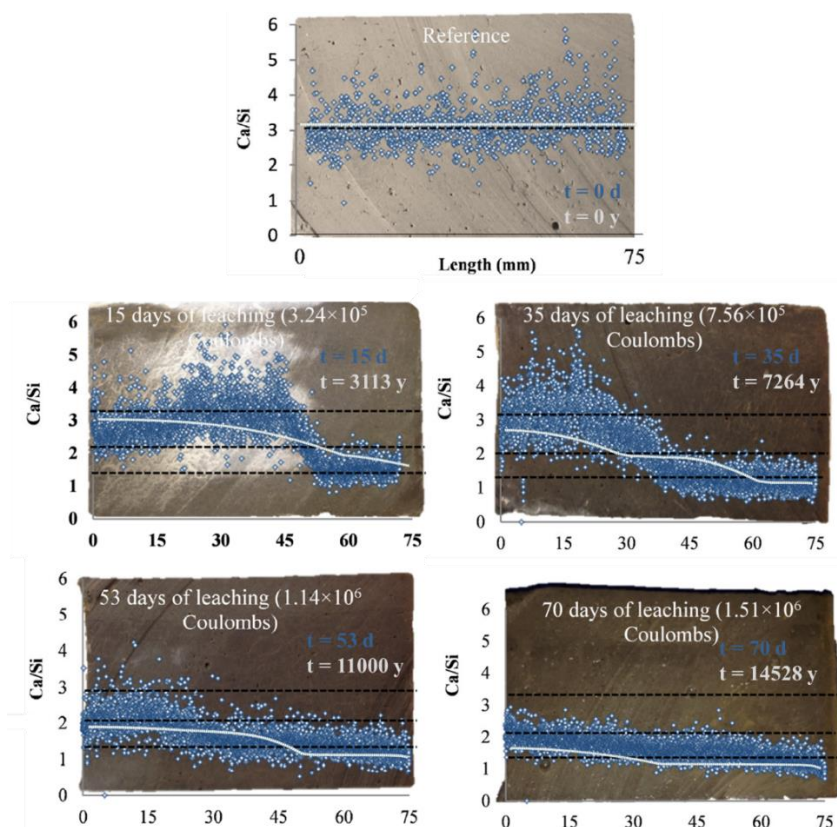


**Figure 2.2.** Axial profiles of Ca/Si ratio in cement paste specimens obtained at different times from laboratory experiments (blue dots, Babaahmadi et al., 2015) and the chemo-mechanical model (grey lines). Times in blue and light grey correspond to experimental data and model results, respectively. Horizontal dimension in mm.

**Table 2.1.** Young's modulus of concrete, mortar and HCP before and after leaching and % decrease obtained experimentally (Babaahmadi et al., 2015) and with the model.

Sample		Initial Young's modulus (GPa)	Leached Young's modulus (GPa)	Chemical damage
Concrete	HCM Model	42.6	20.3	0.524
	Experimental	46.5	24.1	0.482
Mortar	HCM Model	37.7	13.2	0.649
	Experimental	30.4	15.2	0.501
HCP	HCM Model	26.6	5.95	0.776
	Experimental	11.4	6.24	0.453

**Table 2.2.** Compressive and tensile strength of concrete samples for intact and aged states: comparison between experiments (Babaahmadi et al., 2015) and model results.

Concrete sample	Compressive strength (MPa)		Tensile strength (MPa)		Effective diffusion coefficient aged/intact ratio
	Intact	Aged	Intact	Aged	
HCM Model	43.17	16.98	10.20	4.37	4.05
Experimental	43 ± 0.3 <sup>1</sup>	12.7 ± 0.1 <sup>1</sup>	10.2 ± 0.1 <sup>1</sup>	2.8 ± 0.1 <sup>1</sup>	> 3.94 <sup>2</sup>

## 2.4 CONCLUSIONS

A multi-scale chemo-mechanical model for cementitious materials has been implemented in iCP to simulate the degradation of transport and mechanical properties of cement paste and concrete as a function of the degree of calcium leaching from the samples. Recent experimental data of accelerated calcium leaching tests have been modelled. Comparison of the model with experimental data shows a relatively good agreement. The results of the multi-scale chemo-mechanical model show the impact of long-term interaction with groundwater on the physical properties.

## 2.5 REFERENCES

- Adenot F., Buil M. (1992). Modelling of the corrosion of the cement paste by deionized water. *Cem. Conc. Res.*, 22, 489-496.
- Babaahmadi A., Tang L., Abbas Z., Mårtensson P. (2015). Physical and Mechanical Properties of Cementitious Specimens exposed to an electrochemically derived accelerated leaching of calcium. *Int. J. of Concrete Structures and Materials*, 9(3), 295-306.
- Bary B., Leterrier N., Deville E., Le Bescop P. (2014). Coupled chemo-transport-mechanical modelling and numerical simulation of external sulfate attack in mortar. *Cem. Conc. Comp.*, 49, 70-83.
- Camps G. (2008). Etude des interactions chemo-mécaniques pour la simulation du cycle de vie d'un élément de stockage en béton. PhD Thesis Paul Sabatier Univ. Toulouse, France.
- Gérard B., Pijaudier-Cabot G., Laborderie C. (1998). Coupling diffusion-damage modelling and the implications on failure due to strain localisation. *Int. J. Solids Struct.*, 35, 4107-4120.
- Heukamp F. H., Ulm F.-J., Germaine J. T. (2005). Does calcium leaching increase ductility of cementitious materials? Evidence from direct tensile tests. *J. Mater. Civ. Eng.*, 17, 307-312.
- Idiart A., Coene E. (2016). Chemo-mechanical modelling of calcium leaching experiments in cementitious materials. In 1<sup>st</sup> Annual Workshop Proc. CEBAMA, Barcelona, Spain, 11-13 May.

- Idiart A., Shafei B. (2016). Modelling of concrete degradation - Hydro-chemical processes. Report for the safety evaluation SE-SFL. Swedish Nuclear Fuel and Waste Management Co. SKB R-16-18 (in press).
- Lothenbach B., Le Saout G., Gallucci E., Scrivener K. (2008). Influence of limestone on the hydration of Portland cements. *Cem. Conc. Res.*, 38, 848-860.
- Mazars J. (1986). A description of micro- and macroscale damage of concrete structures. *Engineering Fracture Mechanics*, 25(5–6), 729-737.
- Mazars J., Hamon F., Grange S. (2015). A new 3D damage model for concrete under monotonic, cyclic and dynamic loadings. *Materials and Structures*, 48, 3779–3793.
- Nardi A., Idiart A., Trincherio P., de Vries L. M., Molinero J. (2014). Interface COMSOL-PHREEQC (iCP), an efficient numerical framework for the solution of coupled multiphysics and geochemistry. *Computers & Geosciences* 69, 10-21.
- Peerlings R. H. J., de Borst R., Brekelmans W. A. M., de Vree J. H. P. (1996). Gradient-enhanced damage for quasi-brittle materials. *Int. J. for Numerical Methods in Engng.*, 39, 3391-3403.
- Stora E., Bary B., He Q.-C., Deville E., Montarnal P. (2009). Modelling and simulations of the chemo–mechanical behaviour of leached cement-based materials: Leaching process and induced loss of stiffness. *Cem. Conc. Res.*, 39, 763-772.
-

### 3 BRGM/ P. Leroy, S. Gaboreau, F. Claret (BRGM), J. Lützenkirchen and F. Heberling (KIT), S. Huisman and E. Zimmermann (FZJ)

#### Abstract

Concretes have remarkable properties that explain why they are used for the storage of nuclear wastes in geological formation. These properties are their very basic pH, high surface charge density, and very high specific surface area that slow down radionuclides migration in porous media. However, concretes are also very reactive and their reactive transport properties are complex due to the different minerals composing them. Electrical measurements are non-intrusive methods that are sensitive to the movement of electrical charge through the porous medium. These measurements can bring very useful information on concrete's reactivity. However, they have to be accompanied by a multi-scale modelling approach to be correctly interpreted. Here, we show the modelling work performed for interpreting streaming potential and complex conductivity measurements on low-pH concrete samples. After a literature review, the electrostatic surface complexation model of Haas and Nonat (2015) has been chosen to describe the surface electrical properties and particularly the zeta potential of the Calcium Silicate Hydrate (C-S-H) phase composing concretes and the complex conductivity model of Leroy et al. (2008) has been extended to mixtures of monovalent and multivalent ions in the pore water. This last work will be published shortly in Geophysical Journal International (Leroy et al., 2017).

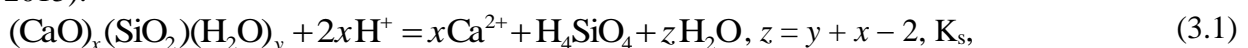
**Keywords:** low-pH concretes, electrical properties, surface complexation reactions, streaming potential, complex conductivity, models.

#### 3.1 METHODOLOGY

The approach chosen in the modelling of the surface electrical properties of low-pH concretes (pH  $\leq 11$ ) is the following. First, the streaming potential measurements on low-pH concretes (that will be performed in 2017) will be interpreted in terms of zeta potential and ion concentrations at the mineral/water interface using an electrostatic surface complex model. This surface complexation model describes the surface electrical properties of the C-S-H phase, which is assumed to be the main mineral phase controlling the electrical properties of concretes (because of its very high specific surface area). Second, the ion concentrations at the mineral/water interface deduced from the surface complexation model will be used to interpret the complex conductivity measurements on low-pH concretes (that will be performed during 2017). The complex conductivity model of Leroy et al. (2008) has also been extended to consider the presence of multivalent and monovalent ions at the mineral/water interface, in order to interpret the complex conductivity measurements on low-pH concretes.

#### 3.2 ELECTROSTATIC SURFACE COMPLEXATION MODEL

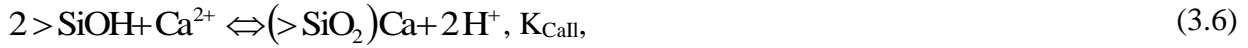
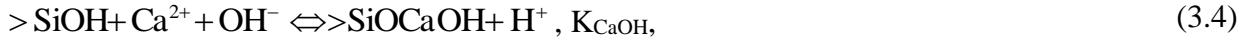
The surface complexation model of Haas and Nonat (2015) has been chosen to compute the surface electrical properties of low-pH CSH ( $\alpha$ -CSH, Ca/Si ratio between 0.75 and 1) and concretes (pH  $\leq 11$ ). This electrostatic surface complexation model considers (1) the solubility of the CSH phase in water, (2) the deprotonation of the silanol surface sites ( $>SiOH$ ) at the surface of CSH and (3) the exchange of  $H^+$  by  $Ca^{2+}$  ions at the surface of the silanol surface sites. The solubility reaction and the two surface complexation reactions are written as (Haas and Nonat, 2015):





where  $K_s$  is the solubility constant (or product), which depends on the type of C-S-H, and  $K_{\text{SiOH}}$  and  $K_{\text{SiOCa}}$  are the equilibrium constants associated with the surface complexation reactions (log $K_s = 53.5$ , log $K_{\text{SiOH}} = -9.8$  and log $K_{\text{SiOCa}} = -7$  for  $\alpha$ -C-S-H, Haas and Nonat, 2015).

Haas and Nonat (2015) also considered the following surface complexation reactions for C-S-H:



where  $K_{\text{CaOH}}$ ,  $K_{\text{bridging}}$ , and  $K_{\text{Call}}$  are the equilibrium constants for the sorption of  $\text{CaOH}^+$  species, dissolved silica species, and of  $\text{Ca}^{2+}$  ions by silanol surface sites in the interlayer space of CSH, respectively (log $K_{\text{CaOH}} = -9$ , log $K_{\text{bridging}} = 2.2$  and log $K_{\text{Call}} = -11.4$  for  $\alpha$ -CSH, Haas and Nonat, 2015).

The surface complexation model of Haas and Nonat (2015) was developed using PHREEQC, and was used to compute the zeta potential of C-S-H as a function of the  $\text{Ca}^{2+}$  concentration in water, by assuming that the zeta potential is located at the same plane than the plane where deprotonation of silanol surface sites occurs. In addition, in the PHREEQC code of Haas and Nonat (2015), the addition of a new silicate on the bridging is forbidden. The different silanol sites were therefore differentiated in the coding depending on whether they are on a pairing or a bridging tetrahedron, on internal or external surfaces.

The fitting of the zeta potential measurements (according to electrophoretic mobility measurements on C-S-H suspensions) using the surface complexation model of Haas and Nonat (2015) is relatively good (Figure 3.1), but the surface complexation model of Haas and Nonat (2015) does not consider a capacitance to describe the electrical potential behaviour between the surface of C-S-H (where deprotonation of the silanols surface site occurs) and the Stern plane containing adsorbed counter-ions such as  $\text{Ca}^{2+}$  ions. We propose to improve their surface complexation model by considering a capacitance between the surface of C-S-H and the Stern plane. Furthermore, we also have to extend their surface complexation model by considering the sorption of  $\text{Na}^+$  ions in the Stern layer of C-S-H. We will use the basic Stern model of Leroy et al. (2013) for silica nanoparticles to implement the surface complexation model of Haas and Nonat (2015). We can also use the work of Viallis-Terrisse et al. (2001) and Elakneswaran et al. (2009) to extend the surface complexation model of Haas and Nonat (2015), considering the sorption of  $\text{Na}^+$ ,  $\text{Cl}^-$  and  $\text{SO}_4^{2-}$  ions in the Stern layer of C-S-H.

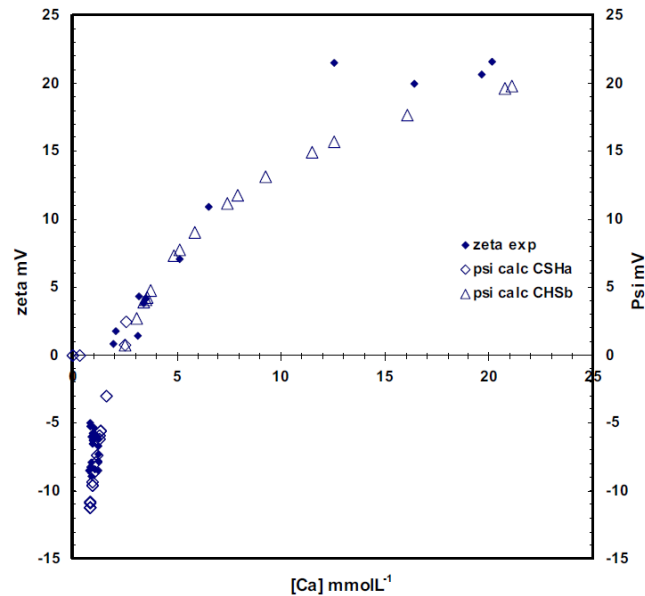


**Figure 3.1.** Zeta potential of C-S-H suspensions (from Haas and Nonat, 2015).

### 3.3 COMPLEX CONDUCTIVITY MODEL

When pH and alkalinity increase, calcite frequently precipitates and hence modifies the petrophysical properties of porous media. The complex conductivity method can be used to directly monitor calcite precipitation in porous media because it is sensitive to the evolution of the mineralogy, pore structure and its connectivity. We have developed a mechanistic grain polarization model considering the electrochemical polarization of the Stern and diffuse layer surrounding calcite particles. Our complex conductivity model depends on the surface charge density of the Stern layer and on the electrical potential at the onset of the diffuse layer, which are computed using a basic Stern model of the calcite/water interface. The complex conductivity measurements of Wu et al. (2010) on a column packed with glass beads where calcite precipitation occurs are reproduced by our surface complexation and complex conductivity models. The evolution of the size and shape of calcite particles during the calcite precipitation experiment is estimated by our complex conductivity model (Figure 3.2). At the early stage of the calcite precipitation experiment, modelled particles sizes increase and calcite particles flatten with time because calcite crystals nucleate at the surface of glass beads and grow into larger calcite grains around glass beads. At the later stage of the calcite precipitation experiment, modelled sizes and cementation exponents of calcite particles decrease with time because large calcite grains aggregate over multiple glass beads, a percolation threshold is achieved, and small and discrete calcite crystals polarize. This last work will be published shortly in *Geophysical Journal International* (Leroy et al., 2017).

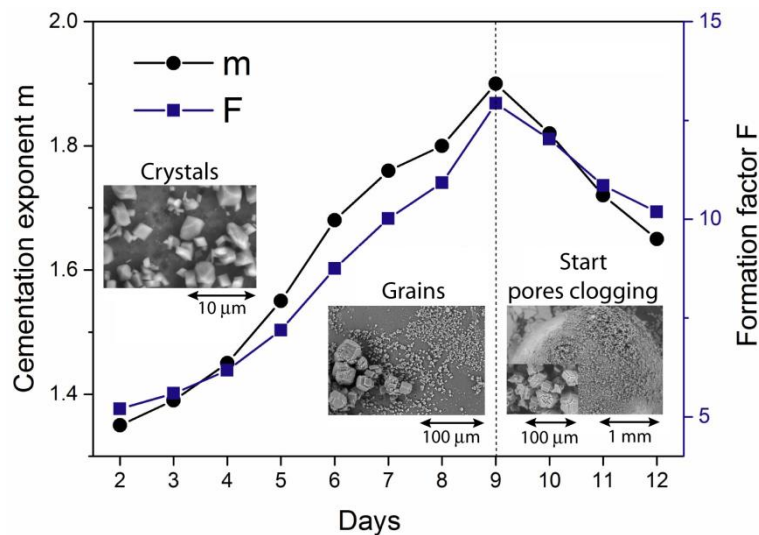


**Figure 3.2.** Computed particles cementation exponent ( $m$ ) and formation factor  $F$  changes during the calcite precipitation experiment of Wu et al. (2010). The cementation exponent and formation factor of the glass beads pack where calcite precipitation occurs have a different trend of changes before and after the starting of the pore clogging (day 9).

### 3.4 REFERENCES

- Elakneswaran, Y., Nawa, T., Kurumisawa, K. (2009). Electrokinetic potential of hydrated cement in relation to adsorption of chlorides. *Cement Concrete Research*, 39, 340-344.
- Haas, J., Nonat, A. (2015). From C-S-H to C-A-S-H: Experimental study and thermodynamic modelling. *Cement and Concrete Research*, 68, 124-138.
- Leroy, P., Revil, A., Kemna, A., Cosenza, P., Ghorbani, A. (2008). Complex conductivity of water-saturated packs of glass beads. *Journal of Colloid and Interface Science*, 321, 103-117.
- Leroy, P., Devau, N., Revil, A., Bizi, M. (2013). Influence of surface conductivity on the apparent zeta potential of amorphous silica nanoparticles. *Journal of Colloid and Interface Science*, 410, 81-93.
- Leroy, P., Li, S., Jougnot, D., Revil, A., Wu, Y. (2017). Modeling the evolution of spectral induced polarization during calcite precipitation on glass beads, accepted to *Geophysical Journal International*.
- Viallis-Terrisse, H., Nonat, A., Petit, J.C. (2001). Zeta-potential study of calcium silicate hydrates interacting with alkaline cations. *Journal of Colloid and Interface Science*, 244, 58-65.
- Wu, Y.X., Hubbard, S., Williams, K.H., Ajo-Franklin, J. (2010). On the complex conductivity signatures of calcite precipitation, *Journal of Geophysical Research-Biogeosciences*, 115, 1-10.

## 7 JUELICH/ S. Rohmen, G. Deissmann, D. Bosbach (JUELICH), B. Shafei, A. Idiart (AMPHOS 21)

### Abstract

Pore-scale models represent an appealing approach for obtaining a more accurate and mechanistic description of physical and chemical processes in heterogeneous porous media such as cement-based materials. For this purpose, a coupled code, which is able to calculate reactive transport processes in porous media on the pore scale using the Lattice-Boltzmann approach, is developed. The current development status and the approaches used to simulate precipitation processes on the pore-scale in a realistic way as a prerequisite to an adequate consideration of the effects of solid phase precipitation on transport properties, such as diffusivity, permeability, porosity, and pore size distribution are described.

**Keywords:** pore-scale modelling, Lattice-Boltzmann-Method, concrete degradation, precipitation processes

### 7.1 INTRODUCTION

Within the scope of CEBAMA, JUELICH and AMPHOS 21 are developing a pore-scale reactive transport modelling framework for the simulation of degradation processes in cementitious materials. Compared to continuum-scale models, pore-scale models represent an appealing approach for obtaining a more accurate and mechanistic description of physical and chemical processes in heterogeneous porous media such as cement-based materials. Reactive transport processes to be addressed with this approach in this project include calcium leaching and carbonation of cementitious systems and their impact on physical properties, such as diffusivity, permeability, porosity, and pore-size distribution. The coupling interface under development combines a transport code based on Lattice-Boltzmann-Method (Palabos) with a geochemical code (PHREEQC). The Lattice-Boltzmann method (LBM) can be used to simulate the microscopic behaviour of particles in a fluid in a discrete way. Space, time and velocity vectors are discretized. By choosing proper discretization steps, mesoscopic and macroscopic properties can be recovered. Thus, LBM can be used to solve e.g. the Navier-Stokes equation for advective-diffusive transport (see Mohamad, 2011; Succi, 2001).

The coupling interface considers the operator splitting approach. In this approach, flow and solute transport are calculated using the LBM at a given time step, followed by the calculation of chemical reactions in PhreeqcRM (Parkhurst and Wissmeier 2015), using the updated species concentrations. In this way, species concentrations and saturation indices for each compound are obtained. The solid phase composition and the porosity values are updated after the chemical step. The fundamentals of the adopted modelling approach and the code coupling have already been described in more detail in Deliverable D3.02 and (Rohmen et al. 2016, in press). Here, on-going developments are described, focusing on the simulation of precipitation processes at pore-scale.

### 7.2 PRECIPITATION AND CRYSTALLIZATION ALGORITHM

Geometrical changes at the microscopic scale due to dissolution and precipitation processes can have a huge impact on the macroscopic hydrodynamic behaviour of the modelled system (Raouf et al., 2013). Changes in pore geometry and transport properties due to precipitation processes depend on the spatial location of precipitated solids, which has to be addressed in the simulations in a proper way. Several nucleation theories have been described in the literature so far (e.g. Kashchiev and van Rosmalen, 2003; Kashchiev, 2000; Prieto, 2014).

---

To mimic the nucleation mechanism for precipitation processes the definition of a crystallisation algorithm is mandatory. This can be achieved by defining different sets of rules and constraints where precipitation is possible and at which point. A simple variant of this was presented by Huber et al. (2014) and refers to the *phase field* technique. In this approach, solids can only precipitate and dissolve at grain surfaces. Translated to the terms of a geochemical simulator as PhreeqC, the target saturation index at grain surfaces is always zero (equilibrium condition). Furthermore, at a distance of more than one spatial step from the grain surface into the pore space no precipitation is possible, allowing supersaturation (non-equilibrium condition). This is translated to a target saturation index of infinity in PhreeqC terminology.

With this kind of approach, the simulation of homogenous nucleation processes is not possible, while precipitation can only occur at grain surfaces which refer to heterogeneous nucleation only. Therefore, a *grain overgrowth* algorithm was implemented by the phase field technique.

In order overcome the lack of homogeneous nucleation effects, the algorithm was extended by taking the distance to the grain surfaces into account. For this purpose, information on the local neighbourhood in the modelling domain is required. This information can be given by a *signed distance field* (SDF) which provides the distances to grain surfaces for all grid node positions. As convention in a SDF, positive values refer to “outside of grain” positions while negative values are representing “inside of grains” positions. In the code, the SDF is implemented by an algorithm called *8SSED* (Leymarie and Levine, 1992). The SDF is updated after each iteration step which involved geometric changes.

With the help of the distance information to grain surfaces, the target saturation index as input for PhreeqC is recalculated. This is done via transfer functions, which can be constructed arbitrarily. For preliminary testing a threshold function consisting of a step located at a threshold distance ( $d_{th}$ ) was implemented. This function is capped at a critical target saturation index value ( $SI_{cr}$ ). The following rule is applied:

$$SI_T(d) = 0 \quad (d \leq d_{th}) \quad (7.1)$$

$$SI_T(d) = SI_{cr} \quad (d > d_{th}) \quad (7.2)$$

Figure 7.1 shows a comparison of three different approaches of defining the target saturation indices in dependency to the grain boundary distance. The flat transformation implements a simple approach at which always equilibrium conditions ( $SI_T = 0$ ) are assumed. In addition, the function used by Huber et al. (2014) and the threshold approaches are plotted.

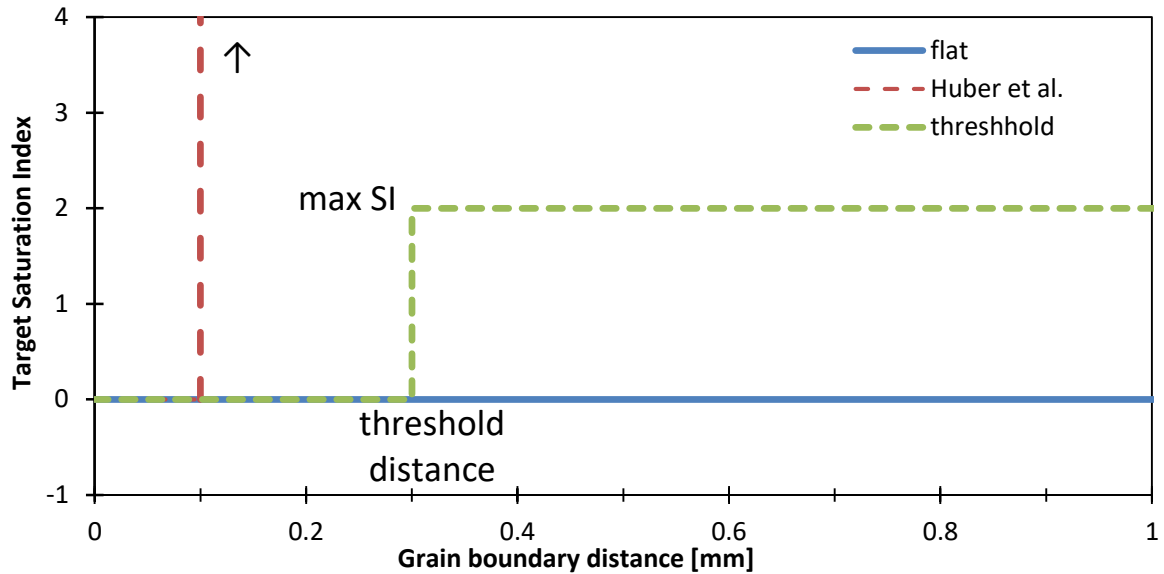


**Figure 7.1.** Comparison of three different variants of target saturation index distance functions in terms of distance to grain boundary. For the function of Huber et al. (2014) a discretization value of 0.1 mm was assumed. For the threshold curve a threshold distance of 0.3 mm and maximum SI of 2 was assumed.

In order to present the effect of the changes made in the precipitation algorithm a qualitative comparison was intended to achieve. Therefore, an input file was generated which is similar to data presented by Tartakovsky et al. (2008). The simulated system consists of two domains of different solutes which lead to the precipitation of a solid phase upon mixing. The modelling domain includes randomly distributed spheres consisting of inert material mimicking the presence of grains. Solutes assumed in the simulation are  $\text{BaCl}_2$  and  $\text{Na}_2\text{CO}_3$  (1 mM), which diffusive mixing leads to the precipitation of witherite ( $\text{BaCO}_3$ ), as shown in Figure 7.2. In contrast to the system addressed by Tartakovsky et al. (2008), no advective flow is considered here. The size of the system was set to  $30 \times 30 \text{ mm}^2$  and discretized in  $300 \times 300$  Lattice-Boltzmann nodes leading to a cell resolution of 0.1 mm. Assuming a diffusion coefficient of  $1 \cdot 10^{-9} \text{ m}^2/\text{s}$  and with this cell resolution, one iteration steps equals 1.666 s.

Simulation results using different transfer functions are shown in Figure 7.3. The simulations were run for 50,000 seconds. The results of the simulation that uses the flat transfer function (always equilibrium case,  $\text{SI}_T=0$ ) shows a broad precipitation zone (Figure 7.3, left), while the threshold transfer function results in precipitation only at the grain surfaces (Figure 7.3, right). A qualitative comparison to the results of Tartakovsky et al. (2008) shows that the distance field based approach is basically capable of providing similar results. Further development steps are required to determine and implement other distance field transfer functions in order to support simulation of different crystallization effects. Depending on the transfer functions the material specific input parameters have to be adjusted. In general, the presented scheme will be used as a starting point to implement algorithms which are capable to model more sophisticated nucleation processes.

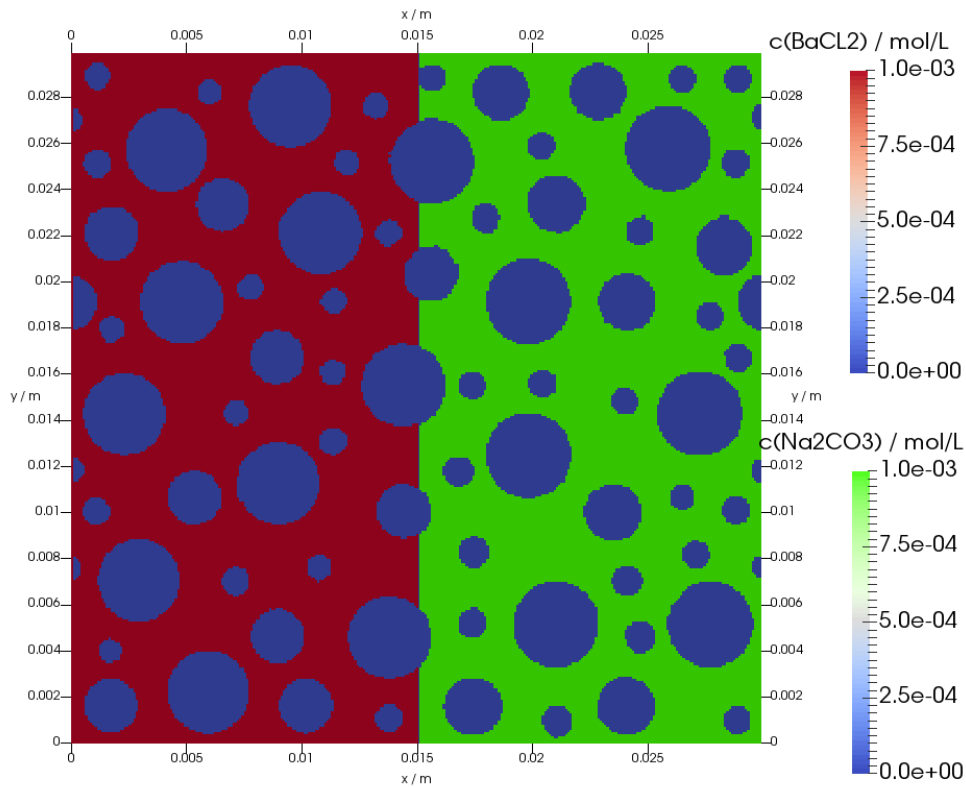


**Figure 7.2.** Initial condition used in the simulation of  $\text{BaCO}_3$ -precipitation. Blue spheres represent a chemically-inert material with a zero diffusion coefficient.

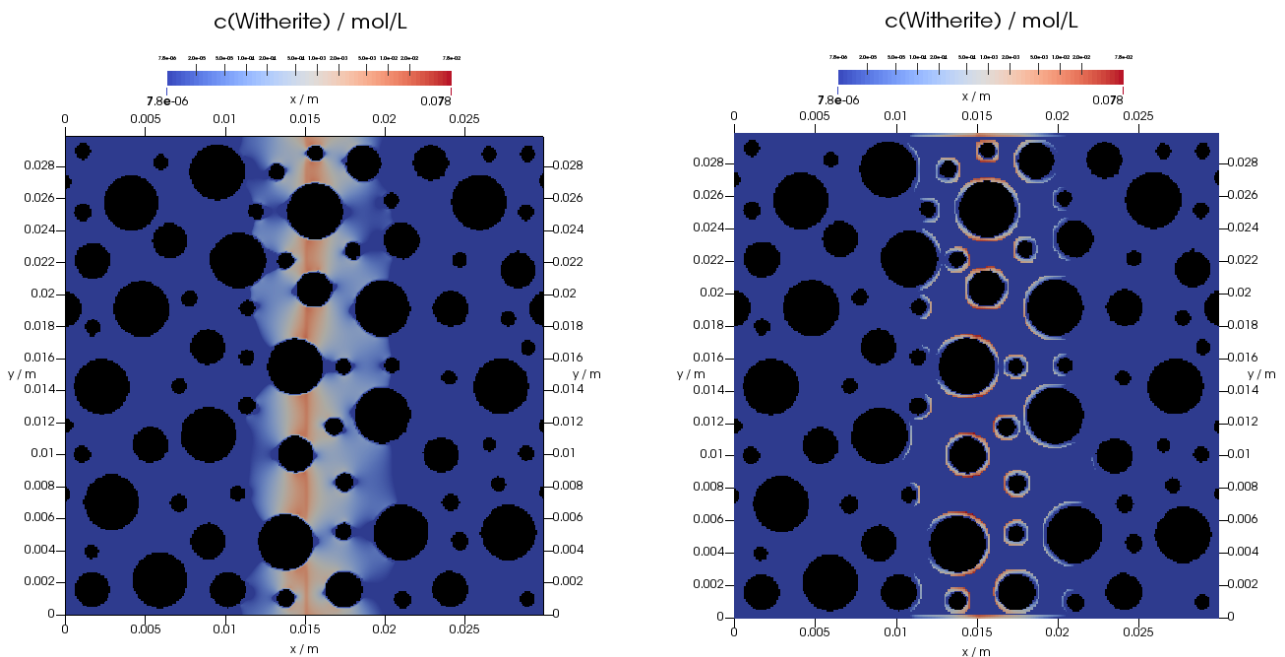


**Figure 7.3.** Solid witherite precipitation after 50,000 seconds (log scale, mol/L). Results for (left) flat target saturation index transfer function and (right) for threshold target saturation index transfer function. Black spheres correspond to non-diffusive inert grains.

### 7.3 CONCLUSIONS AND FUTURE WORK

A coupling code for pore-scale simulations of reactive transport processes based on the Lattice-Boltzmann concept has been developed. Preliminary verification of the code indicates that the tool is appropriate for the simulation of such complex processes. Recently, the code was extended to support the simulation of grain overgrowth precipitation via distance field transformation. An example is presented here that demonstrates the ability to simulate different types of precipitation processes, by means of different transfer functions. Future work includes a comparison of precipitation patterns obtained with the present code with results from other software and experimental data produced within CEBAMA. In particular, the goal is to address the experiments performed by USFD and USURREY within WP1. Until these experimental data are available, it is intended to benchmark the code development against other tools and available experimental data on cementitious materials (e.g. Babaahmadi, 2015) and other heterogeneous porous materials.

### 7.4 REFERENCES

- Babaahmadi A. (2015). *Durability of Cementitious Materials in Long-Term Contact with Water*. Chalmers University of Technology, Göteborg.
- Huber C., Shafei B., Parmigiani A. (2014). A new pore-scale model for linear and non-linear heterogeneous dissolution and precipitation. *Geochimica et Cosmochimica Acta*, 124, 109–130.
- Kashchiev D. (2000). *Nucleation - Basic Theory with Applications*. 1<sup>st</sup> ed. Butterworth Heinemann.
- Kashchiev D., Van Rosmalen G. M. (2003). Review: Nucleation in solutions revisited. *Crystal Research and Technology*, 38, 555–574.
- Leymarie F., Levine M. D. (1992). Fast raster scan distance propagation on the discrete rectangular lattice. *CVGIP: Image Understanding* 55, 84–94.
- Mohamad A. A. (2011). *Lattice Boltzmann Method*. London: Springer London.
- Parkhurst D. L., Wissmeier L. (2015). PhreeqcRM: A reaction module for transport simulators based on the geochemical model PHREEQC. *Advances in Water Resources*, 83, 176–189.
- Prieto M. (2014). Nucleation and supersaturation in porous media (revisited). *Mineralogical Magazine*, 78, 1437–1447.
- Raouf A., Nick H. M., Hassanizadeh S. M., Spiers C. J. (2013). PoreFlow: A complex pore-network model for simulation of reactive transport in variably saturated porous media. *Computers and Geosciences*, 61, 160–174.
- Rohmen S., Shafei B., Idiart A., Deissmann G., Bosbach D. (2016). Pore-scale reactive transport modelling of cementitious systems: Concept development based on the Lattice-Boltzmann method.
- Succi S. (2001). *The Lattice Boltzmann Equation for fluid dynamics and beyond*. Oxford.
- Tartakovsky A. M., Redden G., Lichtner P. C., Scheibe T. D., Meakin P. (2008). Mixing-induced precipitation: Experimental study and multiscale numerical analysis. *Water Res. Res.*, 44, 1–19.
-

### 9.1 SET UP MODEL FOR MIGRATION OF MACRO ELEMENTS IN CONCRETE – BOOM CLAY SYSTEM

Over the reporting period we have implemented a diffusion model for migration in a Boom Clay - Concrete system that is aimed to assist with set up of experimental work by TU-Delft. The cement model includes the latest cement014 database with chemical reactions (EMPA, Lothenbach). The clay model includes equilibrium with charged clay surfaces (Donnan model), organic matter surfaces (NICA-DONNAN model), iron oxides (Generalized 2-layer model), and mineral equilibrium with calcite and pyrite.

The input for this model are the physical and chemical parameters of the clay and concrete sub-systems, and the model calculates concentration profiles in the diffusion system as a function of time.

### 9.2 IMPLEMENTATION OF MULTICOMPONENT DIFFUSION ELECTRO-MIGRATION MODULE IN ORCHESTRA

A multicomponent diffusion / electro-migration module was implemented in the ORCHESTRA modelling framework (Meeussen, 2003). This module takes into account the effect of electric potential on the ion diffusion rates. In contrast with existing implementations this implementation not only allows simplified calculations for zero charge fluxes, but can also calculate ion diffusion rates under given electric potential gradients. The method takes into account individual diffusion coefficients for aqueous species and is fully compatible with existing reactive transport calculations. The module can use concentration or activity gradients as driving force for diffusion.

### 9.3 RESULTS

The new model was evaluated by reproducing the 1D diffusion calculations benchmarks described in the paper by Rasouli et al. (2015). As shown in Figures 9.1 and 9.2, the calculated results agree very well with the reported results, which indicates that the implementation in ORCHESTRA is correct.

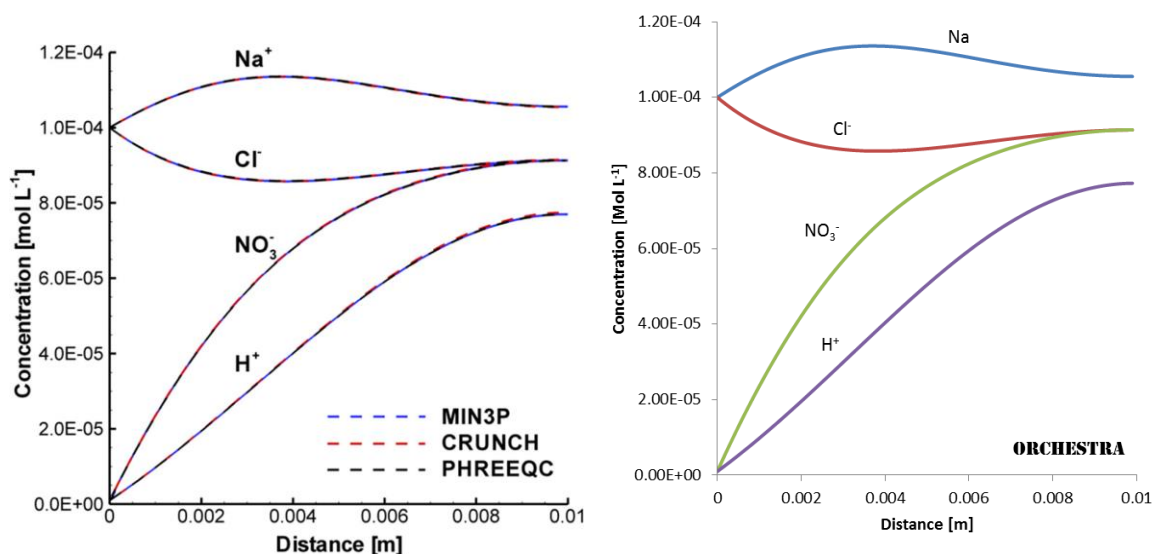


**Figure 9.1.** Comparison of electromigration model results of Benchmark 1 between MIN3P, CRUNCH, PHREEQC (left), and the implementation in the code ORCHESTRA (right).

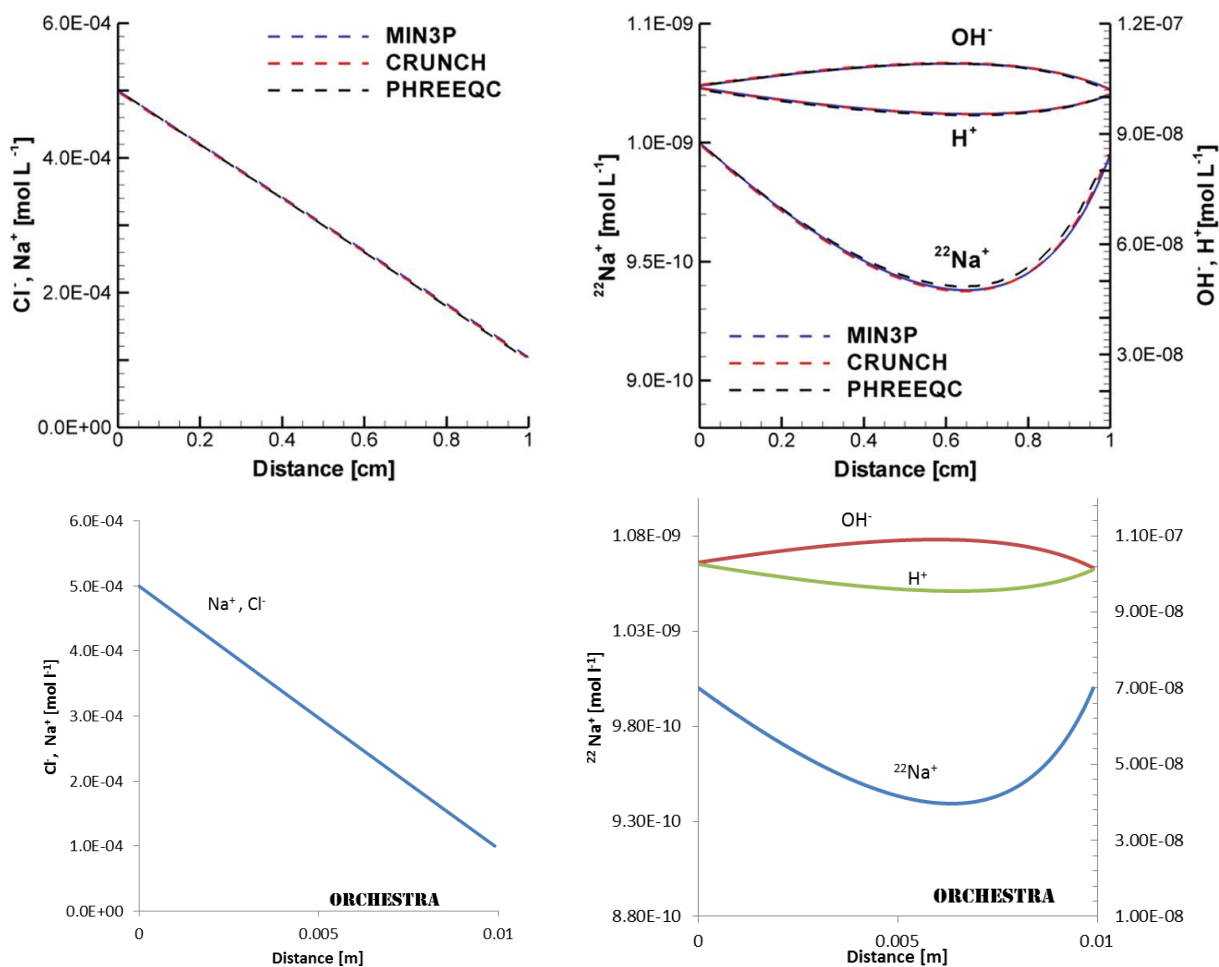


**Figure 9.1.** Comparison of electromigration model results of Benchmark 2 between MIN3P, CRUNCH, PHREEQC (top), and the implementation in the code ORCHESTRA (bottom).

## 9.4 REFERENCES

Meeussen J. C. L. (2003). ORCHESTRA: An Object-Oriented Framework for Implementing Chemical Equilibrium Models. *Environmental Science & Technology*, 37(6), 1175-1182.

Rasouli P., Steefel C.I., Mayer K.U. et al. (2015). Benchmarks for multicomponent diffusion and electrochemical migration. *Comput. Geosci.*, 19: 523. doi:10.1007/s10596-015-9481-z.

## **10 RWMC/ H. Owada, D. Hayashi (RWMC), A. Iizuka (KOBE UNIV.)**

### **Abstract**

The present contribution is based on the S+T contribution to the 1<sup>st</sup> Annual Workshop. On-going work from March 2016 to present will be presented at the 2<sup>nd</sup> Annual Workshop.

Two dimensional (2-D) Hydro-Mechanical-Chemical (H-M-C) coupled calculations with assumptions of various secondary zeolitic minerals were performed to identify the influences of secondary minerals on the change of mechanical and hydraulic properties as the results of long-term alteration of cement-bentonite systems. Analcime, heulandite and clinoptilolite are assumed as the secondary minerals generated by the alkaline alteration of montmorillonite from our previous works and 2<sup>nd</sup> TRU report in Japan (Fujii et. al. (2010) and Japan Nuclear Cycle Development Institute and Federation of Electric Power Company (2007)). Predicted rate of the volume change around waste packages after 10 000 and 100 000 years were largely different by the selection of secondary minerals.

### **10.1 INTRODUCTION**

In the concept of Japanese TRU geological disposal, bentonitic material is anticipated as a mechanical and hydraulic buffer to maintain low water penetration into the disposal vault. Because hydraulic and mechanical properties of bentonitic materials depend on the montmorillonite content and dry density, the dissolution of montmorillonite and precipitation of secondary minerals as a result of the alkaline alteration will directly affect the long term performance of the EBS system. Zeolitic minerals such as analcime, heulandite and clinoptilolite are expected to be secondary phases that will precipitate as a product of cement-bentonite interaction (Fujii et. al. (2010) and Japan Nuclear Cycle Development Institute and Federation of Electric Power Company (2007)). Given that the type of secondary minerals will differ depending on the environmental conditions, such as temperature, groundwater composition, and pH, it is useful to predict the influence of such uncertainty in the current generic phase of the site selection.

### **10.2 MODEL DESCRIPTION AND INPUT DATA**

Dependence of mechanical properties, such as swelling pressure, swelling capacity and compressive strength, and also hydraulic properties, such as water permeability, on montmorillonite content and dry density of bentonitic materials are predicted from the results of previous studies (Sasakura (2002), Ishikawa (1997), Ishibashi (2011) and Takaji (1999)).

Because hydraulic properties such as water permeability and diffusivity change with not only porosity but also montmorillonite content and those affect to the amount of the secondary minerals which are generated by the reaction between bentonitic minerals and cementitious alkaline solution, change of the total volume of the solid phase must be considered to predict the influence of the dissolution of montmorillonite. Morimoto (2014) had formulated such volume change as shown in Figure 10.1.

---

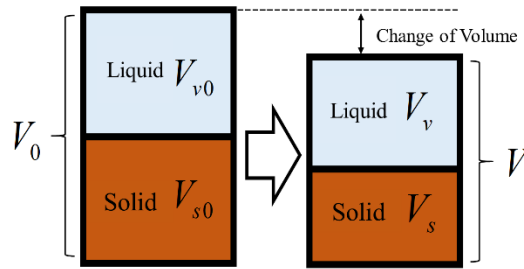


**Figure 10.1.** The Conception diagram of the volume change.

Thermodynamic data from JNC-TDB.TRU (JNC (2005)) and our work (Sato (2017)) are used for the chemical reactions regarding alkaline alteration of bentonitic materials. Data of the density and molar volumes of montmorillonite zeolitic minerals and  $\text{SiO}_2$ , which precipitates as secondary mineral, are listed in Table 10.1.

**Table 10.1.** Density and molar volume of minerals.

Minerals	Density ( $\text{g/cm}^3$ )	Molar volume ( $\text{cm}^3/\text{mol}$ )
Montmorillonite	2.74	138.07
Analcime	2.74	131.5
Clinoptilolite	2.24	361.01
Heulandite	2.20	210
$\text{SiO}_2$	2.65	22.67

Long term chemical-transport calculation was carried out using the code Phreeqc-TRANS to predict the alteration rate ( $\beta$ ) in each element and each time, which is needed to calculate the mechanical properties. Figure 10.2 shows the dimensions, geometric domains, and boundary conditions of the chemical-mass transport coupled calculation.

Initial conditions, such as the distribution of dry density and volumetric strain in buffer materials, were calculated using the code DACSAR-BA which is a Hydro-Mechanical coupling code for clay materials being developed by Kobe University in Japan. Figure 10.3 shows the distribution of the volumetric strain before the chemical alteration.

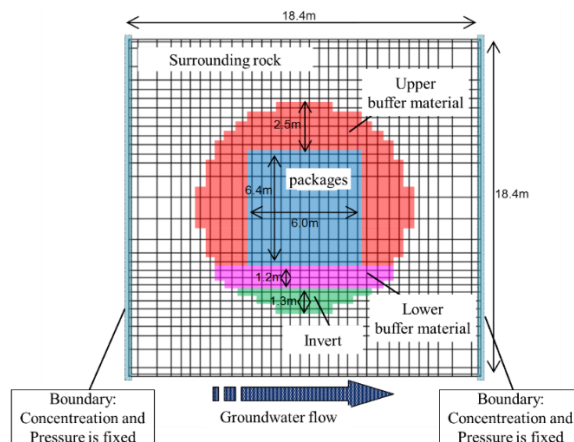


**Figure 10.2.** Geometry of the chemical-mass transport coupled calculation.

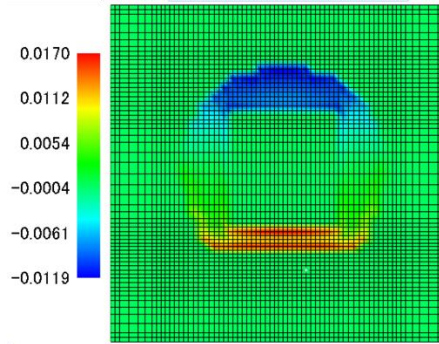


Figure 10.3. Distribution of the volumetric strain (-) before the chemical alteration.

### 10.3 H-M-C COUPLED CALCULATION USING DACSAR-BA

H-M-C coupled calculation is carried out using the code DACSAR-BA. The alteration rate of each position described in the previous section was used for the input to the volume and density calculation for that coupled calculations. To estimate the influence of the different secondary minerals, 4 different calculations were done to consider different scenarios, as shown in Table 10.2.

Table 10.2. Scenarios for the coupled calculations.

Case	Scenario
Case 1	Montmorillonite changed into analcime
Case 2	Montmorillonite changed into clinoptilolite
Case 3	Montmorillonite changed into Heulandite
Case 4 (references)	Montmorillonite dissolves (no secondary minerals)

Figure 10.4 shows the distribution of the alteration rate and rate of volume change in each element. Although the distribution of the alteration rate by the chemical calculation was common in all cases, the volume change was different in each of the scenarios considered. The difference in molar volumes of secondary minerals is considered as the dominant cause of the different volume changes. As shown in Figures 10.5 to 10.7 the distribution of volumetric stress in the buffer strongly depends on the properties of secondary minerals. It is noted that a change in the volume of the buffer will lead to an increase water permeability and diffusivity. This increase is due to the fact that these properties strongly depend on the dry density of the buffer material.

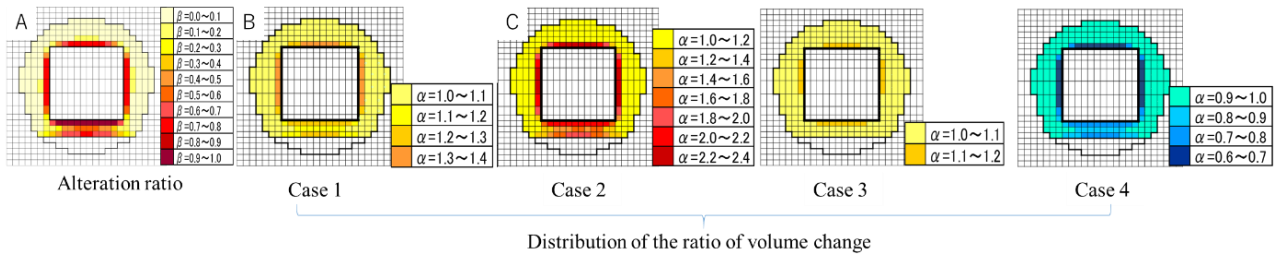
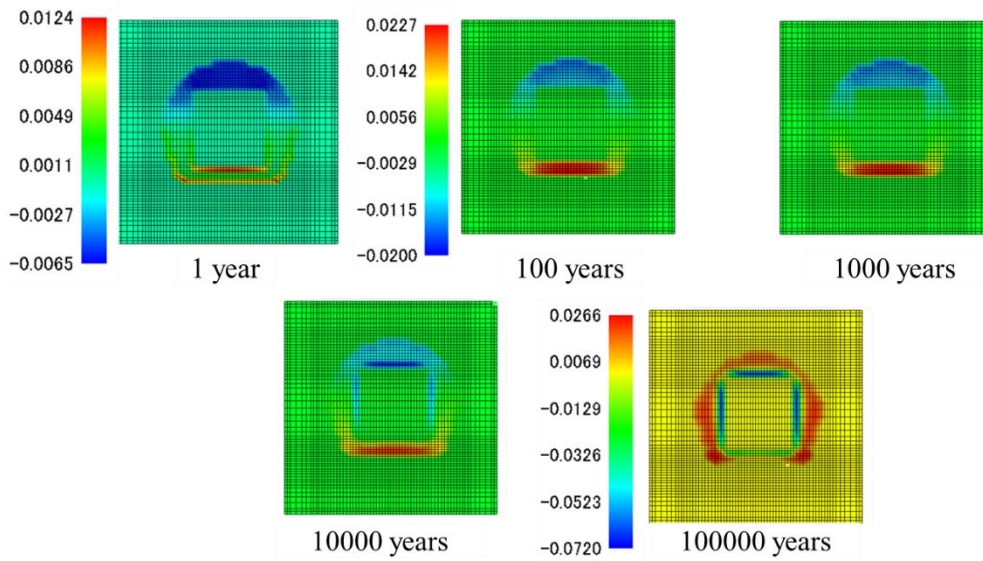
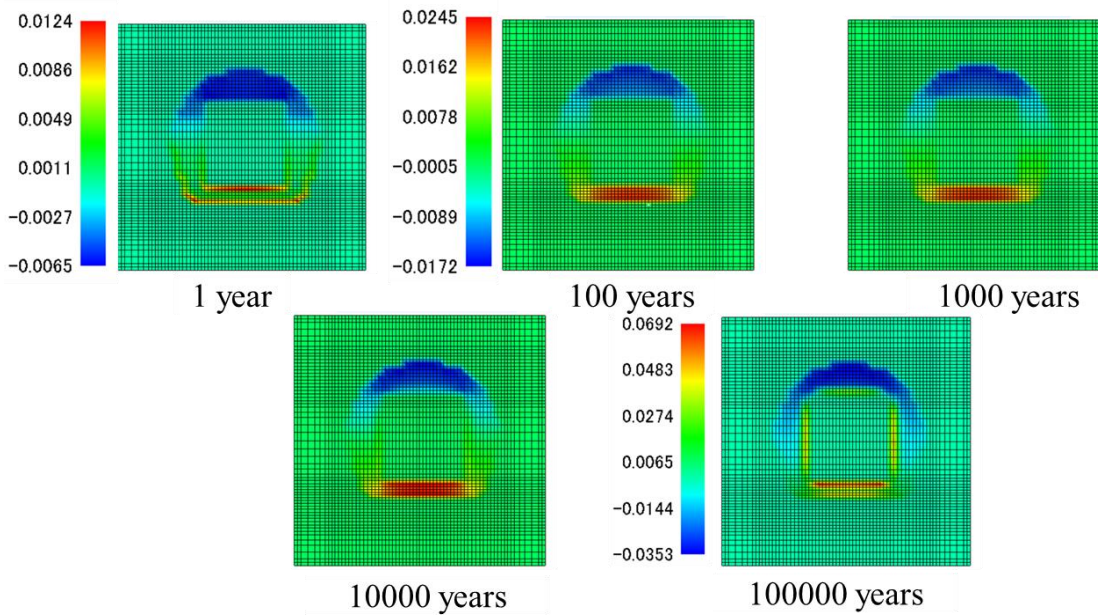


Figure 10.4. Distribution of the alteration rate ( $\beta$ ) and rate of volume change ( $\alpha$ ) in each element.



*Figure 10.5. Distribution of volumetric stress in Case 1 for different times.*



*Figure 10.6. Distribution of volumetric stress in Case 3 for different times.*

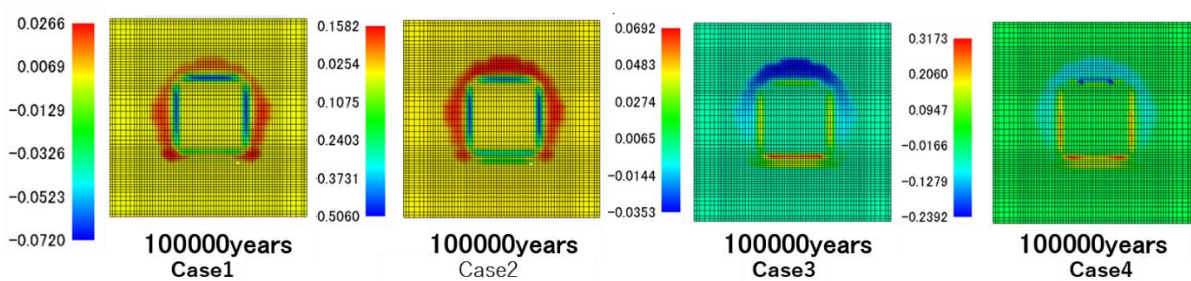


*Figure 10.7. Distribution of volumetric stress at 100000 years later of each cases.*

## 10.4 CONCLUSIONS AND FUTURE WORK

The mineralogy of the secondary minerals will affect the performance of the clay material. To predict the long term performance of the EBS and near field, including cement-clay interactions, it will be important to identify the secondary minerals and to predict the reaction path.

We will perform a long term alteration test for cement-bentonite coupling that will be useful to determine the secondary minerals in the cement-bentonite systems.

## 10.5 REFERENCES

Fujii N., Arcilla C.-A., Yamakawa M., Pascua C., Namiki K., Sato T., Shikazono N., Alexander W.-R. (2010). Natural analogue of bentonite reaction under hyperalkaline conditions: overview of ongoing work at the Zambales ophiolite, Philippines. Proc. 13<sup>th</sup> Int. Conf. on Env. Remediation and Radioactive Waste Mang. (ICEM2010) Tsukuba Japan, 2010/10/3-7.

Ishibashi N., Komine H., Yasuhara K., Murakami S., Mori T., Ito H. (2011). Influences of Monmorilonite content on the compaction properties of bentonite, Proc. 46<sup>th</sup> Conf. Japanese Geotechnical Society (in Japanese).

Ishikawa H., Ishiguro K., Namikawa T., Sugano T. (1997). Compaction Properties of Buffer Material. PNC-TN8410 97-051.

Japan Nuclear Cycle Development Institute and Federation of Electric Power Company (2007). Second Progress Report on Research and Development for TRU Waste Disposal in Japan, JAEA-Review 2007-010, FEPC TRU-TR2-2007-01.

JNC TN8400-2005-010 (2005). Development of Thermodynamic Database for Hyperalkaline Argillaceous Systems (Research Document).

Morimoto K. (2014). Modelling of Mechanical properties of Bentonitic Buffer Materials in Consideration with the Chemical Alteration. Graduation thesis, Kobe University (in Japanese).

Sasakura K., Kuroyanagi M., Okamoto M. (2002). Obtaining the alteration data for the modelling of Bentonite Alteration, JNC TJ8400-2002-025 (In Japanese).

Satoh H. et al. (2017). To be submitted.

Takaji K., Suzuki H. (1999). Static Mechanical Properties of Buffer Material. PNC TN8400 99-041 (In Japanese).

---

## **11 SCK·CEN/ D. Jacques**

The focus of the contribution of SCK to WP3 is on pore-scale modelling of the alterations in concrete during interaction of high-pH cementitious materials and Boom Clay and the effect on effective properties. The objective is to start from experimental information on the microstructure to be obtained in Work Package 1. A three-dimensional coupled reactive transport model based on a lattice Boltzmann approach will be used to simulate solute transport at the pore-scale.

The main focus was on further optimization of the simulation tool previously developed, mainly from the perspective of optimizing the numerical calculations. Unique features of the code are coupling with iPhreeqc which allows for implementing a broad-range of geochemical reactions relevant for simulating the interaction of concrete with Boom Clay. There is a distinction between explicit representation of pores and different solid phases or representation of unresolved pores as a continuum representation with effective transport properties; the latter being relevant to represent C-S-H and its gel pores. Besides using iPhreeqc as a geochemical solver, other solvers can be used – e.g. an abstracted model for leaching and carbonation reactions. At this point, the code which is called YANTRA, can be used starting from input files containing information on the pore structure.

---

**14 UDC/ J. Samper, A. Mon, L. Montenegro, A. Naves and J Fernández (UDC), J. Cuevas and R. Fernández (UAM), M.J. Turrero and E. Torres (CIEMAT)**

**Abstract**

Coupled thermal (T), hydrodynamic (H) and chemical (C) models that account for soil mechanical (m) deformation have been developed for modelling the time evolution of the engineered barrier system (EBS) of a HLW repository. Here we present the modelling results for heating and hydration experiments (HB1, 2, 3, and 4) performed by Ciemat on compacted FEBEX bentonite to study the interactions of concrete-bentonite under repository conditions and analyse how such interactions could affect the bentonite and concrete properties such as porosity. These experiments were performed on concrete and bentonite columns heated at 100°C at the bottom and hydrated at the top. The numerical model reproduces the general trends of the measured water content, porosity, and temperature data and the experimental mineral patterns.

**Keywords:** OP Concrete, bentonite, reactive transport model

**14.1 INTRODUCTION**

The main objectives of UDC in the CEBAMA Project include: 1) improving THCM codes and models of the interactions of concrete and bentonite; 2) performing THCM models of the heating and hydration HB tests; 3) performing long-term predictions of the interactions of bentonite, concrete and clay rock; and 4) contributing to the analysis of time scaling issues. Here we present the THCM model of the HB1, HB2, HB3 and HB4 tests (Turrero et al., 2011; Torres et al., 2013). The tests were modelled with INVERSE-FADES-CORE. The first version of INVERSE-FADES-CORE was developed within FEBEX I and was later improved within the FEBEX II, NFPRO, and PEBS Projects (Zheng et al., 2010; Samper et al., 2013).

**14.2 TESTS AND MODEL DESCRIPTION**

Several sets of tests were performed to study the interactions of concrete and bentonite (Turrero et al., 2011; Torres et al., 2013). The tests aimed at studying the interactions of concrete and bentonite pore water at the conditions prevailing in the EBS during the early hydration stage. This set of tests are denoted as HB and were performed on medium-size cells containing a 7.15 cm thick bentonite sample in contact with a 3 cm thick piece of concrete. The concrete was sulphate-resistant ordinary Portland cement (CEM I-SR) following the recipe by CSIC-IETcc CEM-SR: 400 kg of cement, 911 kg of sand (0-5 mm), and 946 kg of aggregates (6-16 mm) with a w/c ratio of 0.45. Each cell was hydrated at a constant pressure at the top of the cell through the concrete while the temperature was maintained constant at 100°C at the bottom of the cell (Figure 14.1). The HB cells provide data on the concrete and bentonite interface at several times: they were dismantled after 6, 12, 18, 54, and 80 months for the HB1 to the HB5 tests and 104 months for the HB6 test, which will be dismantled within the course of CEBAMA Project. The full set of the experimental results of the HB5 tests are not yet available for modelling. HB1 to HB4 tests were modelled with a 1D grid (see Figure 14.1). Bentonite and concrete parameters were taken from the previous model of the HB4 cell in Samper et al. (2013). The initial porosity of the bentonite is 0.4 and the initial water content is 13.3%, which corresponds to a saturation of 57% and a suction of  $1.27 \cdot 10^8$  Pa. The concrete has a porosity of 0.125 and a gravimetric water content of 2.2%. The initial temperature is 22°C along the cell. Similar to previous THMC models of the FEBEX bentonite (Zheng et al., 2010), the initial total stress is assumed to be uniform, isotropic and equal to 250 kPa. There were experimental problems to maintain a constant water injection pressure during the experiment. Given the lack of reliable

---

water injection pressure data, the injection liquid pressure was estimated from measured cumulative inflow data. Its value is equal to 100 kPa.

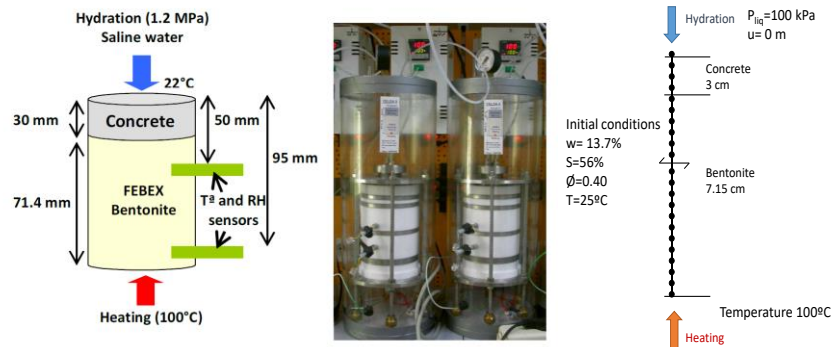


**Figure 14.1.** Setup of the concrete-bentonite HB tests (left) on medium-size cells and finite element mesh and boundary conditions for the numerical model (right).

The cells were hydrated with a synthetic Spanish Reference Clay Porewater (Turrero et al., 2011; Torres et al., 2013). The initial composition of the OPC concrete porewater was derived from speciation runs performed with EQ3/6 (Wolery, 1992) by assuming that the concentration of dissolved  $\text{Ca}^{2+}$  is controlled by local chemical equilibrium with respect to portlandite,  $\text{HCO}_3^-$  is at equilibrium with respect to calcite,  $\text{Mg}^{2+}$  with brucite,  $\text{Al}^{3+}$  with ettringite, and  $\text{SiO}_2(\text{aq})$  with C1.8SH (C-S-H with C/S=1.8). The initial mineral volume fractions in the concrete are: 7.4% for portlandite, 2.2% for ettringite, 14.6% for C1.8SH, 1% for brucite, 0.1% for calcite and 62.2% for quartz. Quartz dissolution is small and therefore this mineral is almost a nonreactive phase. The initial pore water composition of the FEBEX bentonite was taken from Fernández et al. (2004). The initial mineral volume fractions in the bentonite are: 0.36% for calcite, 0.08% for gypsum and 1.192% for cristobalite. The smectite was assumed to be not reactive. The model allows the precipitation of the following secondary minerals: sepiolite, C0.8SH, anorthite and anhydrite. The dissolution/precipitation of portlandite, ettringite, C1.8SH, C0.8SH, quartz and cristobalite is simulated under kinetic control (Fernández et al., 2009).

### 14.3 THM MODEL RESULTS

Computed water content and porosity results reproduce the general trend of the measured data at the end of the HB1, 2, 3, and 4 tests (see Figure 14.2). The concrete is fully saturated at 7 days and then, the bentonite hydrates through the concrete. Water content increases near the concrete and decreases close to the heater due to the evaporation. The porosity increases in bentonite interface due to bentonite swelling. The results of the HB1 to HB4 tests are similar because the water intake is fast in the first months and later slows down after 10 months.

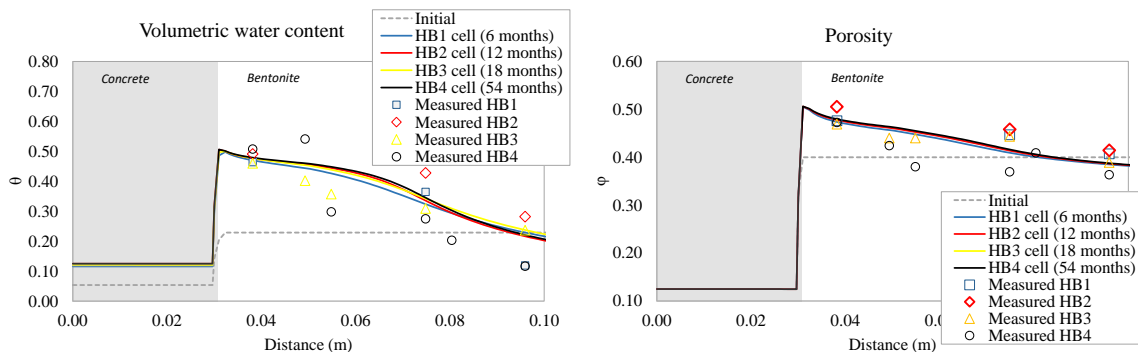


**Figure 14.2.** Computed (lines) volumetric water content (left) and porosity (right) and measured data (symbols) for the HB1, HB2, HB3, and HB4 cells.

## 14.4 CHEMICAL MODEL RESULTS

Figure 14.3 shows the computed mineral volume fractions and pH for the HB1 to HB4 tests. Table 14.1 shows the summary of the main experimental observations on mineral phases at the end of the HB1, HB2, HB3, and HB4 tests and computed results.

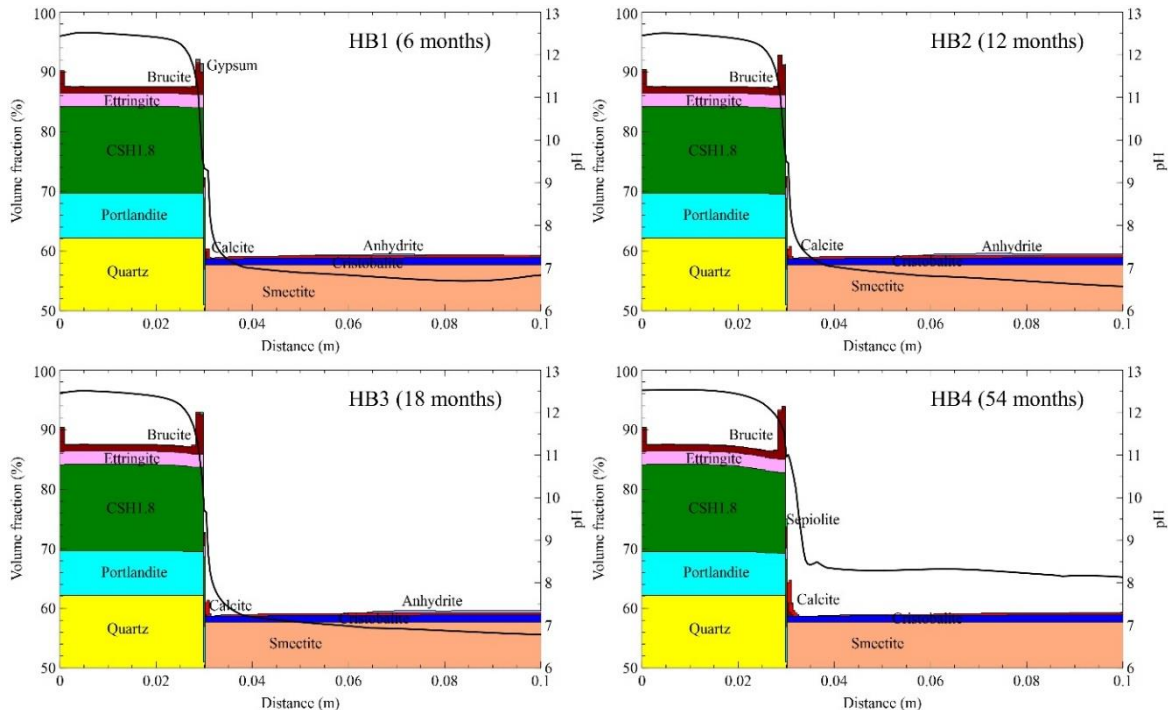


**Figure 14.3.** Computed mineral volume fractions for the HB1, HB2, HB3, and HB4 cells.

These observations are compared qualitatively to the computed values of dissolved/precipitated mineral phases. For the most part, the numerical model captures the main trends of the experimental mineralogical observations. However, there are some discrepancies, especially for ettringite and C-S-H precipitation. For these phases, the numerical model predicts much less precipitation than the observed values. Model discrepancies could be caused by uncertainties in: 1) C-S-H, M-S-H and C-A-S-H phases; 2) kinetic parameters (rate law and specific surface); and 3) the relevant secondary clay minerals. The porosity decreases in the bentonite/concrete interface and at the hydration surface mainly due to the precipitation of brucite and calcite. The front of high pH diffuses into the bentonite. The penetration of the high pH front into the bentonite is 1 cm after 54 months. The diffusion of the alkaline plume is retarded by the mineral precipitation at the bentonite-concrete interface.

## 14.5 CONCLUSIONS AND FUTURE WORK

The results of the THCM model of the HB1, HB2, HB3, and HB4 tests have been presented. The numerical model results reproduce the general trends of the measured water content, porosity, and temperature and the observed patterns of minerals. More adequate representation of C-S-H and M-S-H phases, smectite dissolution, secondary clay minerals, and feedback on porosity changes will be taken into account to improve the model results and reproduce the laboratory observations.

**Table 14.1.** Qualitative comparison of the laboratory observations and model results for the mineral precipitation/dissolution.

	HB1		HB2		HB3		HB4	
	Laboratory observations	Model results	Laboratory observations	Model results	Laboratory observations	Model results	Laboratory observations	Model results
Concrete (Hydration)	Portlandite dissolution	√	Portlandite dissolution	√	Portlandite dissolution	√		
	Calcite precipitation	√	Calcite precipitation	√	Calcite precipitation	√	Calcite precipitation	√
	Brucite precipitation	√	Brucite precipitation	√	Brucite precipitation	√	Brucite precipitation	√
Concrete (30 mm)	Portlandite precipitation	√	Portlandite precipitation	√	Portlandite precipitation	√	Portlandite dissolution	√
	CSH gels precipitation	~	Calcite precipitation in concrete	√	Calcite precipitation in concrete	√	Calcite precipitation in concrete	√
	Quartz precipitation	N	CSH gels precipitation	~	CSH gels precipitation	~	CSH gels precipitation	~
	MSH precipitation	√	Quartz precipitation	N	Quartz precipitation	N	Ettringite precipitation	N
	Zeolites precipitation	NC	MSH precipitation	√	MSH precipitation	√		
			Halite and K-feldspar precipitation	NC	Gypsum and thaumasite precipitation	√		
					Vaterite and aragonite precipitation	NC		
Concrete/bentonite interface (some mm)	Brucite precipitation	√	Brucite precipitation	√	Brucite precipitation	√	MSH precipitation	√
	Portlandite precipitation	N	Portlandite precipitation	N	Portlandite precipitation	N		
	Calcite precipitation	√	Calcite precipitation	√	Calcite precipitation	√	Calcite precipitation	√
	CSH gels (tobermorite and jennite type) precipitation	N	CSH gels (tobermorite and jennite type) precipitation	N	CSH gels (tobermorite and jennite type) precipitation	N	CSH gels (0.8) precipitation	N
	Smectite alteration not observed	NC	Ettringite precipitation	N	Ettringite precipitation	N	No Ettringite precipitation	√
			Gypsum precipitation	√	Gypsum precipitation	√		
		Smectite alteration (brucite saponite-smectite mixed phase <sup>2</sup> )	NC	Smectite alteration (brucite saponite-smectite mixed phase <sup>2</sup> )	NC			
Bentonite	Unaltered bentonite mineralogy	~	Unaltered bentonite mineralogy	~	Unaltered bentonite mineralogy	~	Calcite dissolution	√
							Gypsum and chloride precipitation	√

## 14.6 REFERENCES

- Fernández A.M., Bayens B., Bradbury M., Rivas P. (2004). Analysis of pore water chemical composition of a Spanish compacted bentonite used in an engineered barrier. *Phys. Chem Earth* (29), 105-118.
- Fernández R., Cuevas J., Mäder U. K. (2009). Modelling concrete interaction with a bentonite barrier. *Eur. J. Mineral.*, 21, 177-191.
- Samper J., Mon A., Montenegro L., Pisani B., Naves A. (2013). Report on testing multiple-continua THCM models with laboratory and large-scale tests. Deliverable 3.4-1 of the PEBS Project.
- Torres E., Turrero M.J., Escribano A., Martín P.L. (2013). Geochemical interactions at the concrete-bentonite interface of column experiments. Deliverable 2.3-6-1 of PEBS Project.
- Turrero M.J., Villar M.V., Torres E., Escribano A., Cuevas J., Fernández R., Ruiz A.I., Vigil de la Villa R., del Soto I. (2011). Laboratory tests at the interfaces, Final results of the dismantling of the tests FB3 and HB4. Deliverable 2.3-3-1 of PEBS Project.

Wollery T.J. (1992). EQ3/3. A software package for geochemical modeling of aqueous system: package overview and installation guide version 7.0. UCRL-MA-110662-PT-I, LLNL, Livermore, California.

Zheng L., Samper J., Montenegro L., Fernández A.M. (2010). A coupled model of heating and hydration laboratory experiment in unsaturated compacted FEBEX bentonite. *J. Hydr.*, 386, 80-94.

**Abstract**

As a first step towards realistic modelling of engineered barriers for Performance Assessment and CEBAMA experiments modelling, geochemical calculations of bentonite dissolution in model cement-leach aqueous solution have been performed using PHREEQC. Bentonite dissolution is expected to be the most significant chemical process when bentonite and cement materials will come to direct or indirect contact (each through the direct contact with groundwater). For a preliminary study, the bentonite was considered to be an ideal solid solution of Mg-/Na-/Ca-/K-Montmorillonites (3:1:1:1 molar ratio), based on the cation distribution in exchange capacity, CEC, of the Czech commercial bentonite BaM. Moreover, interaction with hydrated cement was idealized as an equilibration with alkaline water with composition similar to cement leachates (represented by dissolution of portlandite and NaOH). Influences of phase ratio  $m/V$ , temperature and pH were studied.

**Keywords:** cement, montmorillonite, solubility, phases, portlandite, PHREEQC.

**16.1 METHODOLOGY**

For this study, PHREEQC version 3.3.7 (Parkhurst and Appelo, 2013) has been used with the ThermoChimie SIT 9.0b thermodynamic database (Giffaut et al., 2014; Ciavatta, 1980; Guggenheim and Turgeon, 1955) at a fixed pe value of 4. The bentonite has been modelled as an ideal solid solution of Mg-/Na-/Ca-/K-Montmorillonites (3:1:1:1 molar ratio, corresponding to the distribution of cations in CEC of the Czech commercial product BaM (Červinka et al., 2016)). For its properties see Table 16.1, the effective molecular weight  $M_{\text{eff}} = 446.1 \text{ g}\cdot\text{mol}^{-1}$ . The model of aqueous cement leaching is based on dissolution of portlandite (for  $\text{pH} \leq 12.4$ ) and NaOH (for  $\text{pH} > 12.4$ ) in groundwater from PVP Bukov – underground laboratory (synthetic groundwater composition in (Červinka et al., 2016) as SGW2).

**Table 16.1.** Formulae and molecular weights ( $M$ ) of Metal-Montmorillonite ( $Me\text{-}Y$ ) models used, the  $Y$  part in the formulae is  $Mg_{0.34}Al_{1.66}Si_4O_{10}(OH)_2\cdot 4.45H_2O$ . The dissolution reaction for  $Me\text{-}Y$  is of the form (1), where  $z$  equals to 1 or 2 corresponding to the charge of a metal ion.

Name	Formula	$M$ [ $\text{g}\cdot\text{mol}^{-1}$ ]
Mg-Y	$Mg_{0.17}Y$	443.6
Na-Y	$Na_{0.34}Y$	447.2
Ca-Y	$Ca_{0.17}Y$	446.2
K-Y	$K_{0.34}Y$	452.5



**16.2 RESULTS**

On Figure 16.1 the phase ratio dependences of dissolved bentonite molar amount are shown for pH values from 12.0 to 13.5 at temperature  $T = 25 \text{ }^\circ\text{C}$ . As supposed, the solubility increases with solution alkalinity. The parameter  $\varphi$  is defined as ratio of phase and standard phase ratios  $\varphi = (m/m_w) / (n_0 \cdot M_{\text{eff}} / m_{w,0})$ , where  $n_0 = 6 \text{ mol}$  ( $= 3+1+1+1$ ) and  $m_w = m_{w,0} = 1 \text{ kg}_w$  (the higher dissolved amount means the more negative value of  $\Delta n$ , the dissolved mass equals  $-M_{\text{eff}} \cdot \Delta n$ ). The dissolved molar amount of montmorillonite in  $1 \text{ kg}_w$  ( $-\Delta n$ ) limits to the true solubility value (phase ratio independent) for  $\varphi$  large enough ( $\varphi > 30$ ). For all further studies,  $\varphi = 5000$  has been used.

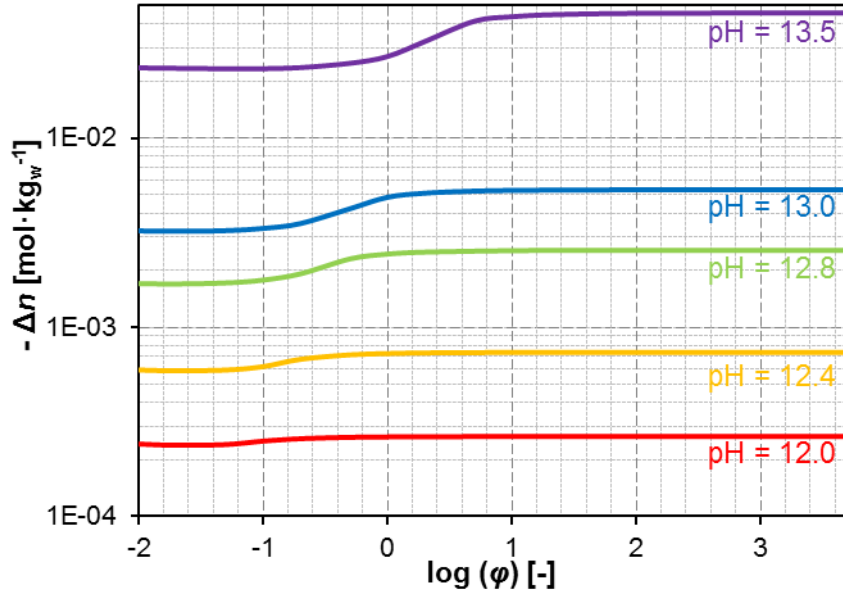


**Figure 16.1.** Dependence of dissolved molar amount of Montmorillonites ( $-\Delta n$ ) on phase ratio parameter  $\phi$  and pH at  $T = 25^\circ\text{C}$ .

The solubility dependence on pH and temperature is presented below in Figures 16.2 and 16.3 respectively. The quadratic trend for logarithm of solubility has been found as appropriate to formulas (2) and (3) and respective fitting parameters for a few representative fixed  $T$  and pH values tabulated Table 16.2.

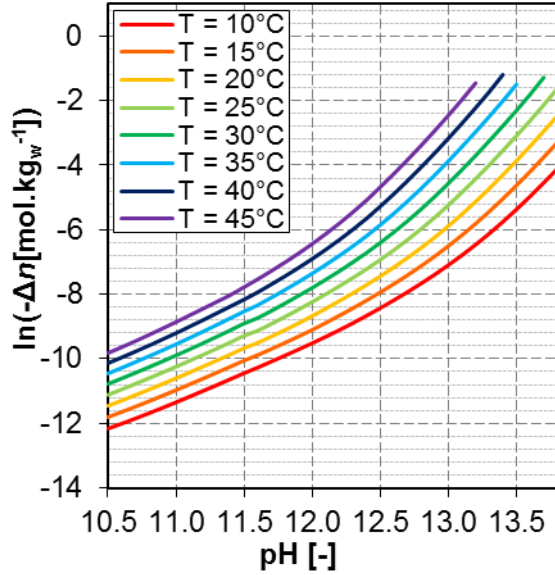


**Figure 16.2.** The  $-\Delta n$  as a function of pH.

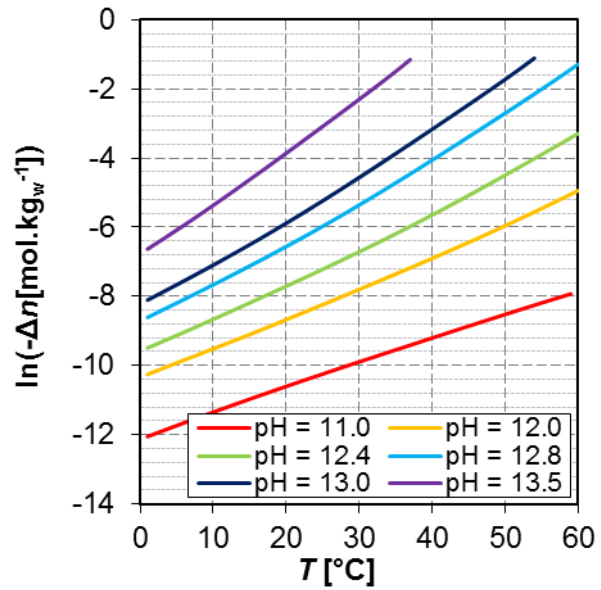


**Figure 16.3.** The  $-\Delta n$  as a function of  $T$ .

$$\ln\left(-\frac{\Delta n}{\text{mol}\cdot\text{kg}_w^{-1}}\right) = a_0(T) + a_1(T)\cdot(\text{pH} - \text{pH}_0) + a_2(T)\cdot(\text{pH} - \text{pH}_0)^2, \quad (16.2)$$

$$\ln\left(-\frac{\Delta n}{\text{mol}\cdot\text{kg}_w^{-1}}\right) = b_0(\text{pH}) + b_1(\text{pH})\cdot(T - T_0) + b_2(\text{pH})\cdot(T - T_0)^2, \quad (16.3)$$

where  $T_0 = 25^\circ\text{C}$ ,  $\text{pH}_0 = 12.4$ .

**Table 16.2.** Fitted values of parameters  $a_i$  and  $b_i$  in formulas (2) and (3).

$T$ [°C]	$a_0(T)$ [-]	$a_1(T)$ [-]	$a_2(T)$ [-]	pH [-]	$b_0(\text{pH})$ [-]	$b_1(\text{pH})$ [K <sup>-1</sup> ]	$b_2(\text{pH}) \cdot 10^4$ [K <sup>-2</sup> ]
15	-8.14	2.68	0.447	11.0	-10.25	0.072	1.13
20	-7.65	2.85	0.505	12.0	-8.25	0.087	1.81
25	-7.15	3.04	0.559	12.4	-7.22	0.101	3.14
30	-6.63	3.21	0.597	12.8	-5.96	0.120	4.03
35	-6.09	3.38	0.620	13.0	-5.23	0.130	4.12
40	-5.55	3.58	0.658	13.5	-3.09	0.157	3.59

### 16.3 CONCLUSIONS

Solubility of Montmorillonite ideal solid solution in model cement leach has been found to increase with both temperature and pH in the respective ranges 10-60 °C and 10.5-13.8. This upward trend can be approximated by formulas (2) and (3). The developed model description will help by interpretation of results of real experiments performed in WP1 by UJV and CTU-CEG.

### 16.4 REFERENCES

- Ciavatta L. (1980). The specific interaction theory in the evaluating ionic equilibria. *Ann. Chim. (Rome)*, 70, 551–562.
- Červinka R., Vopálka D., Adam R., Baborová L., Brázda L., Drtinová B., Hofmanová E., Kittnerová J., Rosendorf T., Štamberg K., Vetešník A. (2016). Transport of radionuclides from the repository / input parameters and process model for assessing the transport of radionuclides through engineering barriers (2<sup>nd</sup> interim report). SÚRAO Technical Report 51/2016, in Czech.
- Guggenheim E.A., Turgeon J.C. (1955). Specific interaction of ions. *Trans. Faraday Soc.* 51: 747–761.
- Giffaut E., Grivé M., Blanc P., Vieillard P., Colàs E., Gailhanou H., Gaboreauc S., Marty N., Madé B., Duro L. (2014). Andra thermodynamic database for performance assessment: ThermoChimie. *Applied Geochemistry*, 49, 225–236.
- Parkhurst D.L., Appelo C.A.J. (2013). Description of input and examples for PHREEQC Version 3 — A computer program for speciation, batch-reaction, one-dimensional transport, and inverse geochemical calculations. U.S. Geological Survey Techniques and Methods, book 6, chapter A43, 6-43A.
-

## Abstract

The progress made at VTT during the first 18-months of the four-year project is described. The ongoing studies must be completed before the prediction of Portland cement-based materials dissolution in deep geological nuclear waste repository is possible. At present, there is no method that is able independently to forecast the behaviour of cementitious materials. However, the combination of experimental research and modelling is able to give boundary values for the cementitious materials dissolution in various scenarios.

## 18.1 INTRODUCTION

The pore solution of cementitious materials has a naturally high pH of 13–14. Bentonite backfill and buffer properties are potentially altered by high-pH leachates. A number of nuclear waste managing organizations, such as Posiva (Finland), SKB (Sweden), and NUMO (Japan), have targeted a pH limit  $\leq 11$  for cementitious leachates. It has been suggested that more natural pH limit would be  $\text{pH} \leq 10$ , as aqueous behaviour of silicates changes. For  $\text{pH} < 10$ , silicates are in neutral  $\text{SiO}_2(\text{aq})$  form in solution whereas for  $\text{pH} > 10$  silicates dissociates to charged species  $\text{HSiO}_3^-$ . Correspondingly, the solubility of quartz increases by three orders of magnitude compared to the pH range 1–10 (Savage, 2007).

The highest tolerable pH of the leachate is 10 or 11 in the bentonite system. Otherwise the long-term stability of the engineered barrier system might be endangered. Mix designs having a leachate with a lower pH than natural pH of 13–14 have been formulated (Cau Dit Coumes et al., 2006, Martino et al., 2011, Vogt et al., 2009, Holt et al., 2014, Holt and Koho, 2016). The low-pH mix designs consist of low alkaline Portland cements mixed with large amounts of pozzolanic materials. Pozzolanic materials are known to react with the hydration products that control the pH of the cementitious materials pore solution. Low-pH materials are still highly basic but the pH value is significantly lower than in traditional Portland cements.

The materials used by VTT were:

1. Ordinary Portland cement from Degerhamn manufactured by Cementa Ab.
2. Granulated silica fume (Parmix supplied by Finnsementti Oy)
3. Blast furnace slag was from Finnsementti Oy
4. Fly ash was from Denmark by E-mineral.
5. Quartz filler purchased from Silbeco Nordic
6. Concrete samples were manufactured using aggregates from ONKALO provided by Rudus Oy.
7. 3 different water compositions (ion-exchanged, saline bentonite porewater and simulated saline groundwater from ONKALO)

## 18.2 DESCRIPTION OF THE MODELLING WORK

Thermodynamic modelling was performed by using Gibbs energy minimization simulation method for calculating chemical equilibria in the experimental system. The software used was GEMS-Selektor v.3, developed by Paul Scherrer Institut. Supplementary database CEMDATA14 was used for cementitious materials together with PSI-Nagra database. GEMS-Selektor software together with CEMDATA14 have been widely used in cement and concrete research. GEMS-Selektor was chosen at this phase of the project because CEMDATA14 database was already built-in the modelling software.

---

The pore solution pH of accelerated paste samples was determined. Three water types were used. Ion exchanged water represents the pore solution pH, whereas saline groundwater sample represents the pH in the vicinity of the concrete structure, when the concrete is exposed to the groundwater. Saline bentonite porewater represents the situation in which the groundwater composition is in equilibrium with bentonite. Modelling of the batch experiments was performed by adding the exact experimental compositions of the used cement together with the used solutions to the model.

### 18.3 RESULTS

In this way, the composition of the pore solution was modelled. Model results of pore solution pH are presented in Figure 18.1 and compared to experimental measurements.

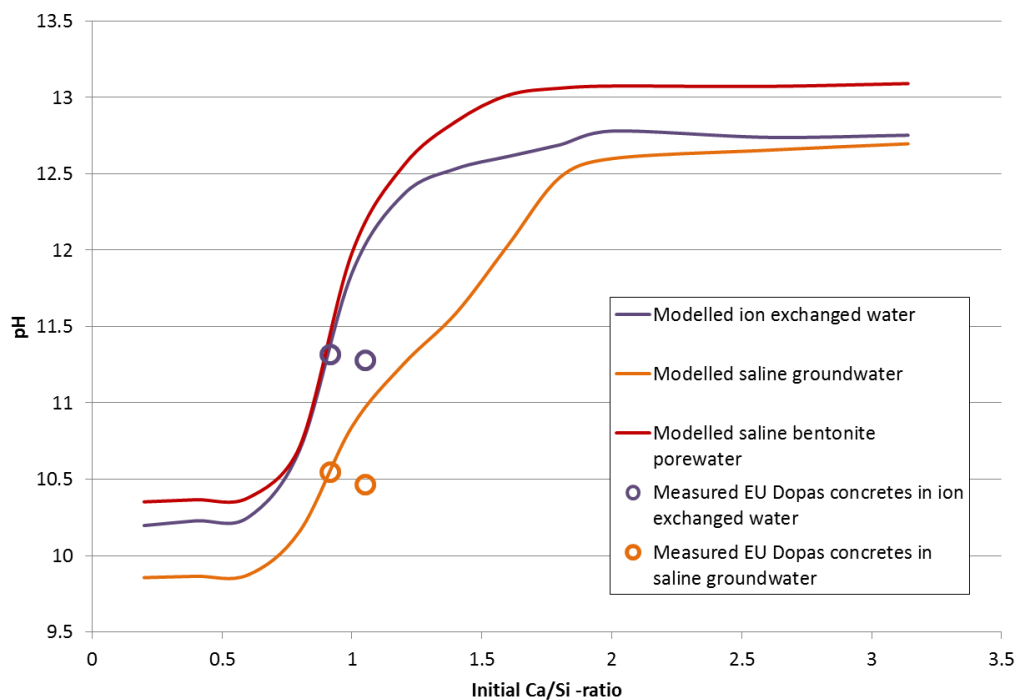


**Figure 18.1.** Experimental and modelled pore solution pH of accelerated paste samples on different water types.

Leaching experiments are still on-going. The modelling of these was performed in a stepwise manner. The exact composition of the leaching samples was modelled and the resulting solid phases were used as input values for the next leaching step. The selected method enabled the comparison between modelled and measured values because the leaching processes in both cases were identical. The modelling and leaching results can be seen in Figure 18.2.

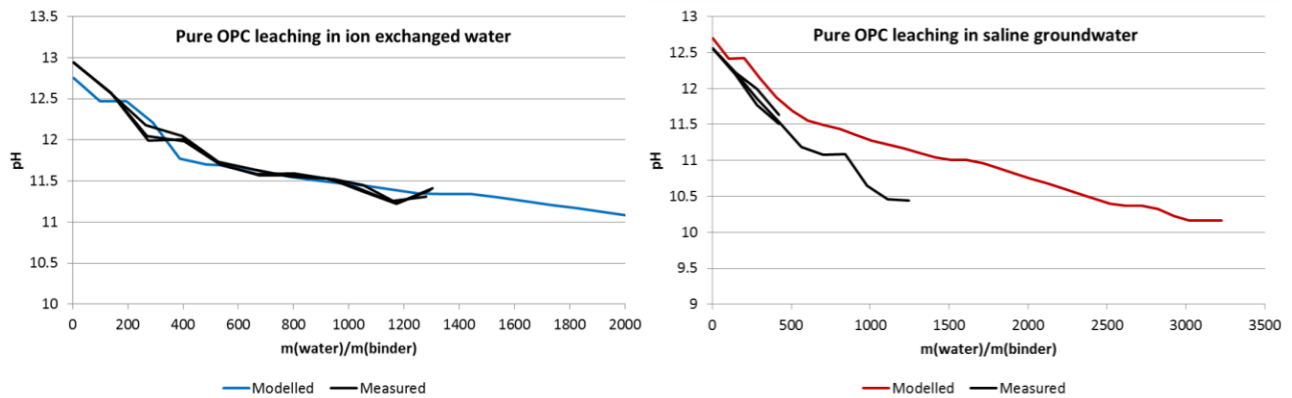


**Figure 18.2.** Modelled and measured leaching of pure OPC in ion exchanged water and saline groundwater.

## 18.4 CONCLUDING REMARKS

There are unsettled questions regarding to the nature of the C-S-H gel and reliability of thermodynamic modelling. These questions may not get the final answer in the current project, but their effect on the uncertainty of the results can be determined. High C/S-ratio C-S-H is either in nanocrystalline form of defect tobermorite or jennite. Although the exact nature of C-S-H form is not known, both of these forms are in equilibrium with solid portlandite which determines the pH at the high C/S-ratios. For C/S-ratios below 0.6, the C-S-H is either solid solution of tobermorite and silica or low C/S-ratio C-S-H. The exact nature of C-S-H at low C/S-ratios is not a necessity to know because the pH of the low C/S-ratio C-S-H can be experimentally obtained. Methods to improve modelling accuracy will be further studied during spring 2017 to better understand the difference with low C/S-ratio between models and the experiments.

There are also uncertainties related to the applicability of thermodynamic modelling. Thermodynamic modelling should be therefore performed with a conservative approach, so that the amount of modelled hydroxyl ions is always equal or greater than the measured values. According to the first modelled leaching results, the selected modelling method seems to do that naturally. Modelled and measured leaching of pure OPC paste in ion exchanged water has good correlation. As the water is changed to more saline, the modelled pH values become greater than the measured values. According to first results, the difference originates from precipitating phases. Even though equilibrium modelling assumes that each phase is fully equilibrated, the measured values have not reached full equilibrium. This tends to lower the solubility of the phases in modelled leaching and causes higher pH values compared to the measured values. Thus, kinetics should be included in the leaching models. This will be attempted later during 2017.

## 18.5 REFERENCES

- Cau Dit Coumes C., Courtois S., Nectoux D., Leclercq S., Bourbon X. (2006). Formulating a low-alkalinity, high-resistance and low-heat concrete for radioactive waste repositories. *Cem. Concr. Res.*, 36(12), 2152–2163.
- Holt E., Koho P. (eds.) (2016). DOPAS Deliverable D4.5 POPLU Experimental Summary Report. 170 p. available from <http://www.posiva.fi/en/dopas/deliverables>.
- Holt E., Leivo M., Vehmas T. (2014). Low-pH concrete developed for tunnel end plugs used in nuclear waste containment. In Concrete Innovation Conference (CIC 2014), 11-13 June, Oslo, Norway.

Martino J., Dixon D., Holowick B., Kim C.-S. (2011). Enhanced sealing project (ESP) Seal Construction and Instrumentation. NWMO report.

Savage D. (2007). Low pH Cements, SKI Report 2007:32.

Vogt C., Lagerblad B., Wallin K., Baldy F., Johansson J.-E. (2009). Low pH self compacting concrete for deposition tunnel plugs. Swedish Nuclear Fuel and Waste Management Co. SKB report R-09-07.

---

**Abstract**

During the past period, the LML team has worked on constitutive modelling of hydromechanical behaviour of concrete fractures. Existing laboratory data from the doctoral thesis by Yang (2011) at the University of Lille have been used. An elastic-plastic model has been formulated together with the description of fracture permeability evolution under both normal compression and direct shearing.

**Keywords:** concrete fracture, normal compression, direct shear, hydromechanical behaviour, constitutive modelling, permeability evolution

**20.1 ELASTOPLASTIC MODEL**

Based on the experimental data presented above, an elastoplastic model is proposed in this section for the description of mechanical behaviour of concrete fractures subjected to normal stress, shear stress and fluid pressure.

Under the normal stress, the mechanical behaviour of fracture is described by a nonlinear elastic model (Bandis and al., 1983). The normal stiffness of fracture is a function of relative normal displacement. Furthermore, the effect of fluid pressure inside fracture is taken into account by extending the Terzaghi’s effective stress concept to saturated concrete fracture. In Figure 20.1, the numerical fitting of the nonlinear elastic model against experimental data in a normal compression test on a concrete fracture is presented.

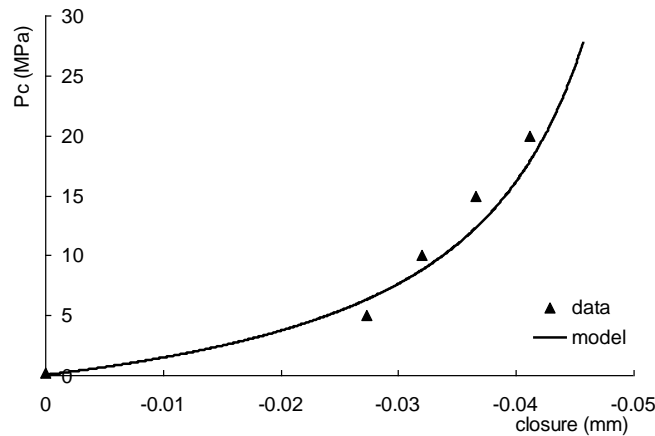


**Figure 20.1.** Numerical simulation of nonlinear stress-strain curve in normal compression test of concrete fracture and comparison with experimental data.

In a shear test under a given normal stress, both normal displacement and shear displacement are produced and coupled. An elastoplastic model is then proposed. Each component of displacement is divided into an elastic part and plastic part. The elastic deformations are characterized respectively by the normal and shear stiffness, which are functions of fracture opening or compaction. The plastic deformations are described by a non-associated plastic model. A generalized Mohr-Coulomb criterion is proposed as the yield function of fracture:

$$F = (\sigma_n^{eff} \sin \theta + |\tau| \cos \theta) + \tan(\phi_r) (\sigma_n^{eff} \cos \theta - |\tau| \sin \theta) + C_0 \leq 0 \quad (20.1)$$

$\sigma_n^{eff} = \sigma_n + P$  is the effective normal stress.  $\phi_r$  denotes the friction angle and  $C_0$  the cohesion of fracture.  $\theta$  represents the current inclination angle of asperities. Due to the presence of such asperities, the tangential plastic sliding can induce a normal plastic closure or opening. Note that the Mohr-Coulomb criterion adopted for fracture is formally equivalent to the widely used Patton criterion. In order to properly the normal plastic deformation induced by shear stress, a non-associated plastic flow rule is necessary. The following plastic potential is proposed:

$$G = \sigma_n^{eff} \sin\theta + |\tau| \cos\theta \quad (20.2)$$

During the plastic sliding process, asperities of fracture are progressively destroyed. In order to describe this kind of surface evolution, each asperity is idealized by a saw tooth form. The degradation process is represented by a decrease of its inclination angle with the plastic energy,  $w_i^p$ . According to Plesha (1987) the following exponential form is adopted:

$$\theta = \theta_0 \exp(-cw_i^p) \quad (20.3)$$

$\theta_0$  denotes the initial value of asperity inclination angle and the parameter  $c$  controls the rate of asperity degradation. This parameter usually depends on the effective normal stress (Nguyen and Selvadurai, 1998) and the following expression is proposed:

$$c = a \left( \frac{\langle -\sigma_n^{eff} \rangle}{P_{atm}} \right)^b ; a > 0, b > 0 \quad (20.4)$$

where  $P_{atm}$  is the atmosphere pressure.  $a$  and  $b$  are two model's parameters. In Figure 20.2, one shows the numerical simulation of three direct shear test under different normal stresses.

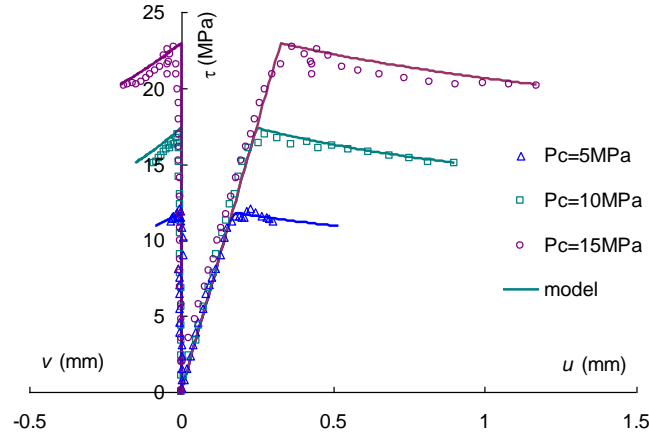


**Figure 20.2.** Numerical simulation of direct shear tests with different normal stresses.

## 20.2 HYDROMECHANICAL COUPLING

For the study of water flow tests, it is assumed that the water flow takes place only along the axial direction. Further, one assumes that the permeability of concrete matrix is much smaller than that of the fracture so that the fluid flow occurs entirely through the fracture. The one-dimensional hydraulic diffusion equation is solved by a finite difference method. The hydraulic conductivity of fracture is a cubic function of normal aperture, and also affected by the fracture surface roughness. The empirical relation proposed by Barton et al. (1985) is used to define the relation between the hydraulic opening ( $e_{hi}$ ) and fracture normal displacement ( $V_i$ ):

$$e_{hi} = \frac{(b_0 + V_i)^2}{JRC^{2.5}} \quad (20.5)$$

The fracture roughness coefficient  $JRC$  is a morphological parameter which is related to the asperity distribution form of fracture. In Figure 20.3, one presents the comparisons between numerical results and experimental data in fluid injection tests into concrete fractures under different values of normal stress.

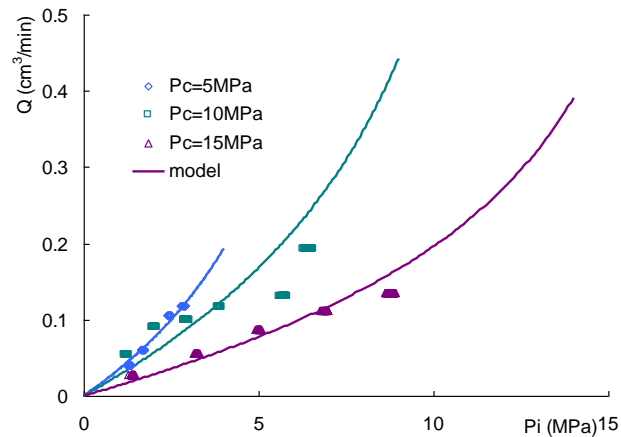


**Figure 20.3.** Comparison between numerical results and experimental data for fluid flow rate with injection pressure.

### 20.3 REFERENCES

- Bandis S., Lumsden A., Barton N. (1983). Fundamentals of rock joint deformation, *Int. J. Rock Mechanics and Mining Science*, 20, 249-268.
- Barton N., Bandis S., Bakhtar K. (1985). Strength, Deformation and Conductivity Coupling of Rock Joints. *Int. J. Rock Mech. Min. Sci. & Geomech.*, 22, 121-140.
- Nguyen T.S., Selvadurai P.S. (1998). A model for coupled mechanical and hydraulic behavior of a rock joint. *Int. J. Numer. Anal. Methods Geomech.*, 22, 29-48.
- Plesha M.E. (1987). Constitutive models for rock discontinuities with dilatancy and surface degradation, *Int. J. Numer. Anal. Methods. Geomech.*, 11, 345-362.
- Yang H. (2011). Experimental investigation and numerical modelling of hydromechanical behaviours of concrete under various loading conditions, Doctoral thesis (in French), University of Lille, France.

#### **Acknowledgements:**

This study was jointly funded by ANDRA (French National Agency for radioactive waste management) through the grant number 51992 and the European Commission through the project CEBAMA (grant number 662147). The authors declare that they have no conflict of interest.

### Abstract

The work of Paul Scherrer Institute (PSI) concentrated on the development of a new reactive transport code utilizing the Nernst-Planck approach for transport of ions in the presence of an electric field in combination with the Gibbs Energy Minimization approach for solving geochemical equilibria. In this document, we present benchmark calculations for testing the numerical implementation of the Nernst-Planck equations.

**Keywords:** transport modelling, diffusion, Nernst-Planck equations, electrochemical diffusion

### 24.1 INTRODUCTION

Our task is the development of new reactive transport software using the most advanced conceptual and numerical models to consider electrochemical migration and mineralogical changes. For this purpose, we use state-of-the-art well-established tools to solve diffusive transport problems and to calculate geochemical equilibria. The resulting software is going to be able to calculate the diffusion of charged particles under the influence of an electric field, consider the effect of charged mineral surfaces on transport, and compute geochemical reactions including precipitation and dissolution. These reactions can potentially change porosity and related transport parameters of the porous media. Ultimately, the new software will be used to calculate the evolution of clay/cement interfaces considering electrochemical transport of solutes across the interface. In addition, the software can also be used for modelling of accelerated leaching tests where an electric current is used to accelerate diffusion in cement specimen.

### 24.2 IMPLEMENTATION

In a first step, we implemented the so-called Nernst-Planck equations that describe diffusion of ions and other charged complexes in the presence of an electric field. To do so, we use the programming language Python (Python Software Foundation, <https://www.python.org/>). Python is a widely used language in applied math, science and engineering due to its readability, great libraries, no compilation needed, no memory management needed, and finally a growing and supportive community. The transport equations are implemented and solved using FEniCS (Logg, 2012). FEniCS is a scientific tool for solving partial differential equations with several Finite Element based numerical methods. The big advantage of using FEniCS - compared to other existing software packages - is the automated and efficient solution of differential equations, as the user has essentially only to define the weak form of the equation which he would like to solve and FEniCS provides the numerical infrastructure. This allows rapid development and easily adoption of codes. Besides, high-performance computing is supported by FEniCS without rewriting existing codes. For further reading, tutorial, materials and download we refer to [www.fenicsproject.org](http://www.fenicsproject.org).

In a second step, the Reaktoro chemical solver (Leal et al. 2014, 2015, 2016) was coupled into the Nernst-Planck solver. Reaktoro is a framework for modelling chemically reactive systems, and it can interface with PHREEQC (Parkhurst and Appelo, 2013) and GEMS3K (Kulik et al. 2013). Reaktoro also includes on its algorithm the calculation of solid solutions, different activity calculations methods, and the possibility of coupling future implementation methods and functionalities to both Reaktoro and GEMS3K. The transport solver implementation is validated via a benchmark, as described below. The chemical solver is already coupled, but the validation and analysis are still to be done.

---

### 24.3 VERIFICATION

We verified our numerical implementation of the simplified Nernst-Planck equations by comparison with analytical solutions for salt diffusion and by reproduction of a benchmark problem from Lichtner (1994) described as case 1 in Rasouli et al. (2015). This benchmark case calculates the diffusion of  $\text{HNO}_3$  from a low-pH solution ( $\text{pH} = 4$ , right side in Figure 24.1) to a higher pH solution ( $\text{pH} = 6$ , left side in Figure 24.1). Both solutions contain the same elevated NaCl concentrations. The expected diffusion of  $\text{HNO}_3$  from right to left is indicated by an arrow. The chemical system is composed by  $\text{H}^+$ ,  $\text{NO}_3^-$ ,  $\text{Na}^+$ , and  $\text{Cl}^-$ . The initial and boundary conditions are displayed in Figure 24.1. There is a Dirichlet boundary condition with a fixed concentration at  $x = 0$  and an infinite boundary condition on the right side of the container. Results from our implementation are compared to the reference values provided by Rasouli et al. (2015) in Figure 24.2 after a simulation time of 1 hour. We see a very good agreement between the results which verifies our implementation in FEniCS.

Moreover, Figure 24.2 shows an increase in  $\text{Na}^+$  and a decrease in  $\text{Cl}^-$  concentrations which cannot be explained with simple Fickian diffusion models, as there is initially and at the boundaries no concentration difference for NaCl. These effects can only be explained by considering additional cross-coupling terms between charged species. These terms originate from different diffusive mobilities of species and are needed to maintain a charge-balanced solution. The observed concentration variations are sometimes called “uphill diffusion”, although these are only transient phenomena. On the long term the concentrations in the system will equilibrate to the boundary values and will be constant throughout the domain.

Most reactive transport codes cannot reproduce this benchmark, as they apply Fick’s law only and use the same diffusion coefficient for all transported species. This approach also preserves charge balance, but does not take into account the effect of interactions between charged species with different diffusion coefficients.

It should be noted that phenomena similar to “uphill diffusion” might also occur in systems more relevant for the CEBAMA project, i.e. diffusion-driven leaching of cement materials.

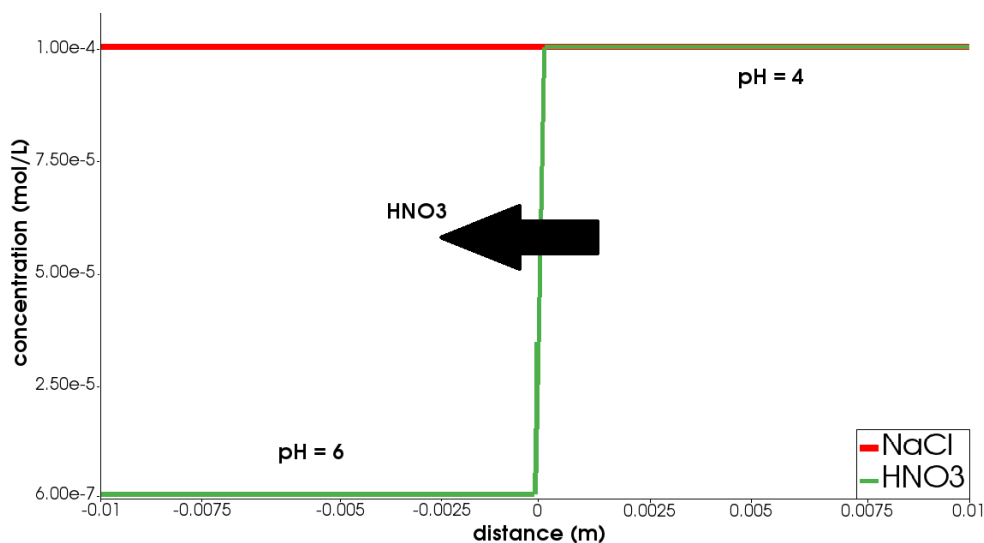


**Figure 24.1.** Initial condition according to benchmark case 1 in Rasouli et al. (2015) with indications of expected ion fluxes due to initial and boundary conditions.

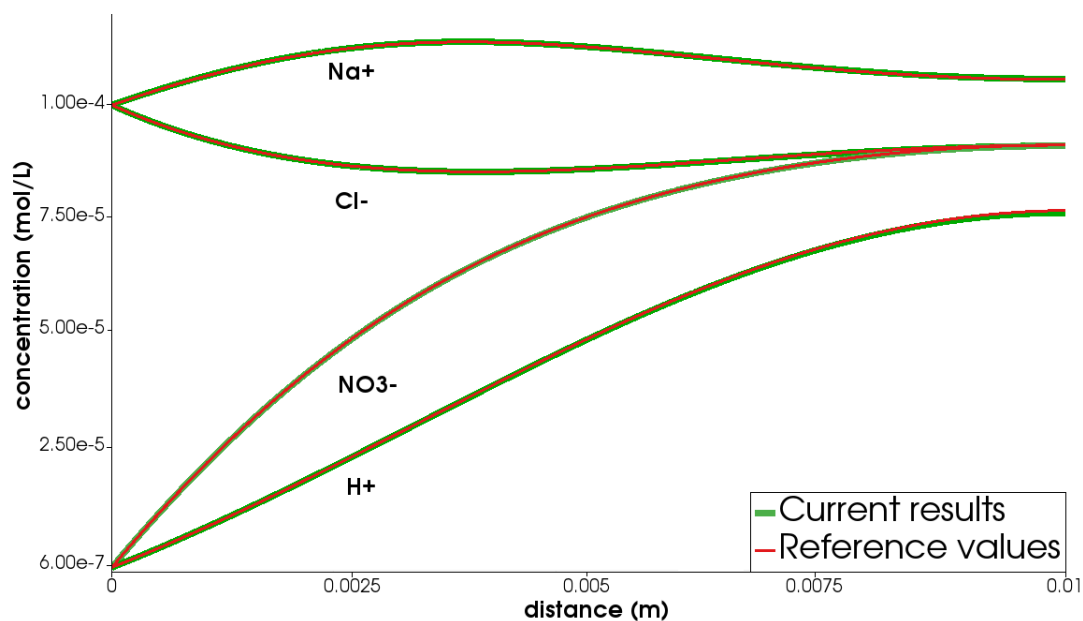


**Figure 24.2.** Comparison between reference values from benchmark case 1 in Rasouli *et al.* (2015) and our results after 1h diffusion time.

## 24.4 REFERENCES

- Kulik, D. A., Wagner, T., Dmytrieva, S. V., Kosakowski, G., Hingerl, F. F., Chudnenko, K. V., Berner, U. R. (2013). GEM-Selektor geochemical modeling package: Revised algorithm and GEMS3K numerical kernel for coupled simulation codes. *Computational Geosciences*, 17(1), 1–24.
- Leal, A. M. M., Blunt, M. J., LaForce, T. C. (2014). Efficient chemical equilibrium calculations for geochemical speciation and reactive transport modelling. *Geochimica et Cosmochimica Acta*, 131, 301–322.
- Leal, A. M. M., Kulik, D. A., Kosakowski, G. (2015). Computational methods for reactive transport modeling: A Gibbs energy minimization approach for multiphase equilibrium calculations. *Advances in Water Resources*, 88, 231–240.
- Leal, A. M. M., Kulik, D. A., Kosakowski, G., Saar, M. O. (2016). Computational methods for reactive transport modeling: An extended law of mass-action, xLMA, method for multiphase equilibrium calculations. *Advances in Water Resources*, 96, 405–422.
- Lichtner, P. C. (1994). Principles and Practice of Reactive Transport Modeling. *MRS Proceedings*, 353, 117.
- Logg, A., Mardal, K.-A., & Wells G. N. (2012). Automated Solution of Differential Equations by the Finite Element Method. Springer.
- Parkhurst, D.L., Appelo, C.A.J. (2013). Description of input and examples for PHREEQC Version 3 – A computer program for speciation, batch-reaction, one-dimensional transport, and inverse geochemical calculations. U.S. Geol. Survey Techniques and Methods, book 6, chapter A43, 6-43A.
- Rasouli, P., Steefel, C. I., Mayer, K. U., Rolle, M. (2015). Benchmarks for multicomponent diffusion and electrochemical migration. *Computational Geosciences*, 523–533.